DOI: 10.1002/ ((please add manuscript number))
Article type: Review

Fiber-based Thermoelectric Generators: Materials, Device Structure, Fabrication, Characterization and Applications

Lisha Zhang[1], Shuping Lin[1], Tao Hua[1], Baoling Huang[2], Shiri Liu[1], Xiaoming Tao[1*]*

[1] Nanotechnology Centre for Intelligent Textiles and Apparel, Institute of Textiles and Clothing, The Hong Kong Polytechnic University, Hong Kong, China

[2] Department of Mechanical and Aerospace Engineering, Hong Kong University of Science and Technology, Hong Kong, China

* Correspondence author: xiao-ming.tao@polyu.edu.hk, tao.hua@polyu.edu.hk

Keywords: flexible thermoelectric generator, fiber, thermoelectric materials, structures, fabrication, characterization

Fiber-based flexible thermoelectric energy generators, being three-dimensionally deformable and light weight, are desirable for applications of large-area waste heat recovery, energy supplier for wearable or mobile electronic systems where both large mechanical deformation, high energy conversion efficiency and electrical stabilities are greatly demanded. They can be manufactured at low or room temperature under ambient conditions by established industrial processes, offering cost-effective and reliable products in mass quantity. This article presents a critical overview and review of the state-of-arts of the fiber-based thermoelectric generators covering their operational principle, materials, structures of devices, fabrication methods, characterization and potential applications. The scientific and practical challenges, critical issues as well as opportunities are also discussed.

1. Introduction

Harvesting scavenging energy can reduce the amount of fuel consumption and fulfil legislation on CO_2 emission.[1] In particular, flexible energy harvesting devices have attracted increasing attention, because they can deform and match three-dimensional contours and large surface areas of objects such as energy sources. Fiber-based flexible generators, in the form of textiles, operating according to triboelectric, piezoelectric and thermoelectric effects, etc..[1-5] are promising candidates to achieve the goal, because their deformability, stretchable, mechanical stability, and light weight enable them to conform to arbitrary curved surfaces like human body and various machine components.[6]

Thermoelectric generators are solid-state devices without moving parts or working fluids, which take advantages of thermoelectric (TE) materials that allow direct energy conversion between thermal and electric forms. According to their deformability, there are two major types of such generators. On one hand, rigid TEGs have been developed and applied for important applications like power generation, refrigeration and temperature sensing.[7] On the other hand, flexible thermoelectric energy generators, being deformable, light and cost effective, have been explored for large-area,[8] waste heat recovery,[9-12] wearable or mobile electronic applications[13-16] where both large mechanical deformation and high electrical stabilities are greatly demanded. Their potentials in personalized microclimate control systems are yet to be explored.

The flexible thermoelectric generators can be further divided into thin-film-based and fiber-based ones. The thin-film TE generators can be bent only over one direction, while the fiber-based TE generators (FTEGs) can accommodate three dimensional deformation due to their excellent tensile, bending and in-plane shear properties thus are more suitable

for above mentioned applications.[6] Large three dimensional mechanical deformation, outstanding fatigue resistance,[3] damage tolerance and high electric stability[13] have been demonstrated by various devices made from fiber assemblies like yarns and fabrics. Moreover, these devices can be manufactured at low or room temperature in ambient conditions by well-established industrial processes, offering cost-effective and reliable products in mass quantity.

Despite of the perceived advantages, the development of FTEGs has met many challenges. Yamamoto and Takai firstly designed and fabricated an FTEG device with metal wires by knitting method in 2002.[17] But the utilization of metal wires as TE materials sacrifices the comfortability of the device. This problem was tackled by Cho's group in 2014.[18] Their FTEG device was fabricated with small TE semiconductor patches that were pressed into woven glass fabric and formed a network like islands in the sea. However, this device can hardly fulfil the demand of flexibility and deformability, in addition, high temperature treatments were required. One-dimensional FTEGs was reported by Shtein's group with metal thin coatings on fibers in 2008.[19] Late on, Kim, Baughman and their colleagues directly fabricated two-dimensional FTEGs by weaving and knitting methods without any rigid substrates.[20]

This article critically reviews the state-of-arts of FTEGs with regard to the increasing demands for renewable energy as well as flexibility and light weight of such devices in large-area or wearable applications. It covers the operational principle, materials, structures of devices, fabrication methods, characterization and potential applications of FTEGs.

Discussions will be presented on the opportunities and challenges in terms of TE materials, device structures, manufacture and applications.

2. Operational Principle of FTEGs

In order to impart flexibility, fibrous materials like fibers, yarns, fabrics or papers can be used as one- or two-dimensional substrates for TE generators. Figure 1(a) shows a typical deformable FTEG draped over a sphere. Coating or lamination are the common routes for fabrication of FTEGs in two dimensional fiber assemblies like fabrics or papers. Alternatively, one may make the p- or n-type legs directly within or on the surfaces of one-dimensional fibers or yarns, as depicted in Figure 1(b).

FTEGs operate on the three TE mechanisms based on Seebeck effect, Peltier effect and Thomson effect. Figure 1 (b) illustrates Seebeck effect, which describes that holes, in p-type semiconductors, which is coated on a yarn, are excited by temperature difference between two ends and move from the hot side to the cold side. If the semiconductors are connected with conductive fabric electrodes, a current will occur as the result of the movement of holes in the TE yarn loop. Peltier effect delineates that if electrical current flows in a loop which consists of p- or/and n-type semiconductors, endothermic or exothermic phenomenon can be observed at the joints. This TE effect is usually used in cooler systems. Thomson effect describes that some heat, except for Joule heat, is absorbed or exuded if temperature gradient exists in a conductor with current. Among the three, Seebeck effect is the fundamental reason why most TEGs can be used to convert heat energy into electrical energy.

The energy conversion efficiency of TE materials is determined by a dimensionless figure-of-merit ZT :

$$ZT = S^2\sigma T / \kappa \quad (1)$$

where S is the Seebeck coefficient, σ is the electrical conductivity, T is the average temperature, and κ is the total thermal conductivity. Lattice vibrations and electron motion make a contribution to the total thermal conductivity which can be expressed by:

$$\kappa = \kappa_l + \kappa_e \quad (2)$$

where κ_l represents the lattice thermal conductivity, κ_e represents the electron thermal conductivity.[21] TE power factor, P , is determined by the Seebeck coefficient and electric conductivity:

$$P = S^2\sigma \quad (3)$$

An ideal TE material should satisfy the following requirements: high Seebeck coefficient and electrical conductivity, and low thermal conductivity. The movement and interaction of electrons and phonons affect TE properties of materials. For semiconductor, electronic properties have a significant influence on Seebeck coefficient and electrical conductivity, while phononic properties on thermal conductivity.[22] The motion of the carriers is determined by the nature of materials and by the mechanism of carriers scattering when they transfer from one place to another.[23] For example, the electrical conductivity, σ , is given by

$$\sigma = ne\mu \quad (4)$$

where n is the carrier concentration, e is the charge on the carrier, and μ is the carrier mobility. Obviously, if the carrier concentration or mobility can be enhanced, electrical conductivity will increase. This will lead to the increment of ZT and power factor, if the Seebeck coefficient does not change too much. However, to improve the *ZT* value is difficult, because of the strong interdependence among the three parameters: S, σ and κ. Electrical conductivity relates to thermal conductivity by the Wiedemann-Franz law:[24]

$$\frac{\kappa_e}{\sigma} = LT \qquad (5)$$

where L is Lorenz number, which is equal to 2.45×10^{-8} V^2/K^2 when heavily doped semiconductors or metals are used Therefore, at a certain temperature, the ratio of κ_e to σ is a fixed value. If electrical conductivity is increased, electronic thermal conductivity should increase. Additionally, the increasing electrical conductivity due to the increment of carrier concentration causes the reduction of Seebeck coefficient.[25, 26]

3. Materials for FTEGs

Selection of appropriate materials is extremely important for design and fabricating FTEGs. TE materials are the central element of FTEGs. These materials should possess high energy conversion efficiency with high carrier mobility and appropriate carrier concentration. Meanwhile, they should own expected thermal and mechanical properties, eco-friendly and stable performance, and easy fabrication process at low or room temperature as well as low cost for materials and manufacture by solution process. Apart from TE materials, electric

connectors and structural pieces are also important elements. The following section will present and discuss the materials that have been studied to fulfil these demands.

3.1. Inorganic TE materials

TE effects can be observed in some conductor and semiconductor materials. In fact, different metals forming thermocouples at their junctions have been used for many years. Although pure metals, like copper, platinum and gold, can be used in thermocouples, metallic alloys are applied more commonly, which can exhibit conductive and semi-conductive properties.[27] Many reviews have thoroughly summarized and prospected recent development and future opportunities of different metallic alloys, metal oxides[28, 29] and metal chalcogenides[30, 31] as TE materials. Semiconductors have been extensively studied and used as the common inorganic TE materials, including Bi–Te alloys, skutterudite compounds, half-Heusler compounds, metal silicide, Ag–Pb–Sb–Te quaternary systems and some high-*ZT* oxides. Here, the former four materials are summarized in Table 1 and discussed below. More comprehensive discussion of others can be found in the literature.[32, 33]

Since the relationship between TE power and composition in bismuth telluride system was reported in 1910 [34] and Bi_2Te_3 was confirmed as a semiconductor in 1955,[35] Bi_2Te_3 and its alloys have been regarded as one of the most ideal TE materials. Nanocrystalline $Bi_xSb_{2-x}Te_3$ bulk alloy has a reported *ZT* of 1.4 at 373K.[36] $Bi_{0.5}Sb_{1.5}Te_3$ with *ZT* of 1.86 at 320K was reported in 2015.[37] The main principle of increase *ZT* value of Bi-Te alloys relies on the reduction of lattice thermal conductivity by dense dislocation arrays, grain

boundaries and point-defect scattering. However, the mobility of carriers will decrease with the decrement of lattice thermal conductivity, which limits the improvement of TE properties. Huang and Kaviany[38] studied molecule dynamics of electron and phonon transport in Bi_2Te_3 systemically to explore theoretical treatment and possibility of obtaining higher *ZT*.

Skutterudite compounds have been pursued, because their crystal structure leads to high electrical conductivity and low thermal conductivity.[39] The structure of skutterudite is a cubic with 32 atoms per cell. Thermal conductivity decreases due to the increment of phonon-scattering centres by arranging atoms in the interstitial voids of this crystal system. It behaves like a phonon-glass and electron-single-crystal (PGEC) material simultaneously.[40] Thermal conductivity of $CoSb_3$-based skutterudite was decreased by substituting Sb with As, caused by the impurity scattering and boundary scattering.[41] Besides, binary skutterudites are novel TE materials due to possessing extremely high carrier mobility. Their TE properties can be improved by filling foreign species into the voids in the molecules, which dramatically affects phonon scattering.[42]

Since Fritz Heusler discovered Cu_2MnAl alloy in 1909, full-Heusler (FH) and half-Heusler (HH) compounds, whose stoichiometry is 2:1:1 and 1:1:1, respectively, have attracted great attention.[43] Especially, HH compounds are semiconducting materials with good electrical and mechanical performance and thermal stability at high temperature.[44] The general formula of HH compounds is ABX, where A and B represent two kinds of transition metals: a rare earth element and a noble metal, respectively, and X is a main-group element.[45, 46] Doping HH compounds with other metal element is an effective method to optimize power

factor and reduce lattice thermal conductivity, because it increases transfer path for carriers and point-defect scattering for phonons.[47] ZrNiSn and FeNbSb based TE materials are regarded as typical HH compounds whose performance is shown in Table 1.[48] A theoretical study of p-type ($FeNb_{1-x}Hf_x$ Sb) and n-type (LaPtSb) HH compound showed that the potential value of *ZT* is 1.42 at 1500K[49] and 2.2 at room temperature,[50] respectively.

The most common metal silicides are Mg_2(Si, Sn)-based materials, which have antifluorite crystal structure. Thermal conductivity of them is much lower than their single compound: Mg_2Si or Mg_2Sn, because of more phonon scattering. Seebeck coefficient of Mg_2(Si, Sn)-based materials can be engineered by controlling the ratio of Mg_2Si /Mg_2Sn to change the bandgap in the alloys. Electrical conductivity of Mg_2(Si, Sn)-based materials can be improved by doping. The *ZT* range of state-of-art Mg_2(Si, Sn)-based materials is from 0.9 to 1.50 at 600K to 800K.[51] More detailed and comprehensive analyse about Mg_2(Si, Sn)-based materials can be found in the literature.[52]

Although the highest *ZT* value of inorganic TE materials have been above 2.5, the measurement was operated at temperature over 900 K.[53] For the application of the conversion of human body heat into electrical energy, TE materials are required to be effective at around 310K. Therefore, although many inorganic materials are good candidates for TE conversion, the most appropriate one at low temperature is the Bi–Te alloys. Furthermore, compared with organic conducting polymers, they are expensive, brittle and often toxic, high temperature is required for fabrication processes which may not be suitable for fiber-based FTEGs.

3.2. Organic TE materials

Comparing to inorganic TE materials, organic ones have many advantages, such as cost-effectiveness, material abundance, low thermal conductivity, light weight, and high flexibility. A variety of polymers have been studied as TE materials, including polyacetylene (PA),[54] polyaniline (PANI),[55] poly(3,4-ethylenedioxythiophene) (PEDOT),[24, 56-64] poly(3-hexylthiophene) (P3HT),[65] polypyrrole,[66] and others. Among them, in contrast to PA with instability to oxidation in atmosphere,[67] semi-conductive polymers like PEDOT and PANI have been intensively explored, because they are stable and easy to fabricate[68] into electronic devices. Additionally, the best TE properties have been reported with poly(styrenesulfonic) acid (PSS)-doped PEDOT.[69] PANI shows high electrical conductivity and low thermal conductivity, because of metallic domains in its structure.[70] However, conducting polymers are limited because of their intrinsic drawbacks like low electrical conductivity and low Seebeck coefficient. Therefore, the *ZT* and power factor of most conductive polymers is in the range of $10^{-2} \sim 10^{-3}$ and $10^{-4} \sim 10^{-6}$ W/(mK^2), respectively.[71] This power factor range is 2 or 3 orders of magnitude lower than those of inorganic TE materials.[71-73] To improve the TE properties of organic conducting polymer, many groups have explored and applied different methods, such as doping and dedoping treatment, hybridizing carbon particles or other inorganic materials, and assembling materials layer-by-layer (LbL). These concentrated efforts aim at the increment of electron concentration and conductivity of polymers,[33] leading to significant progress in TE properties of organic polymer. For instance, the highest power factor at room

temperature was 2710 μW/(mK^2) which was competitive with commercially available Bi_2Te_3.[74]

Although PEDOT has many advantages, such as relatively high electrical conductivity, environmental stability and low density, it is limited by its low electron concentration and low Seebeck coefficient. Besides, for improving the solubility, PEDOT is usually emulsified with PSS in water to fabricate PEDOT: PSS film, or with counterion tosylate (Tos) to PEDOT: Tos. Compared with conducting PANI, semi-conducting PEDOT: PSS and PEDOT: Tos have better TE properties, whose behaviour is similar to bismuth, graphite and telluride alloys. Unlike PANI with a polaron network, PEDOT: PSS and PEDOT: Tos have a bipolaron network thus exhibit better TE properties, because electrical conductivity of metallic PANI decreases with increasing temperature whereas that of semi-metallic PEDOT: PSS and PEDOT: Tos raises with the increment of temperature.[75, 76] The difference of electrical conductivity between metallic and semi-metallic polymers is the result of the distinct location of Fermi level[75] and the dissimilar electronic density of states at the Fermi level.[33] Furthermore, doping the film with dielectric solvents, such as dimethyl sulfoxide (DMSO), ethylene glycol (EG),[69] ammonium formate,[77] *etc.*, can increase the electrical conductivity by several orders of magnitude, as the solvents align the PEDOT chains to increase mobility and help carriers hopping because of the reduced hopping distance.[78] There are two functions of these solvents: (1) the hydrophobic PEDOT phase is conversed, for the hydrophilic PSS phase is partly separated from the composite by these hydrophilic solvents; (2) more connections among PEDOT phases are formed, for these solvents modifies the morphology of the polymer.[26] The maximum *ZT* at room temperature was 0.42, which was measured from the DMSO-doped PEDOT: PSS

films.[69] Except for doping method, post-treatments, such as adding solvents[79, 80] or dedoping,[81] were explored. Dedoping treatment of the PEDOT: PSS nanofilms was reported to removed excess PSS chains and forming neutral PEDOT chains, leading to the increment of Seebeck coefficient and electrical conductivity and the decrease of thermal conductivity along the cross-plane direction. The lower thermal conductivity is caused by two factors: one is the change of nanostructure, and another is that PEDOT: PSS with less PSS owns more van der Waals bonds than covalent bonds.[78] After the treatment, although the *ZT* was only approximate 0.1, the power factor was as high as 112 μW/(mK^2).[81] Furthermore, multilayer thin films were fabricated for the first time by layer-by-layer (LbL) depositing process in 2015.[82] Because the LbL process was attributed to highly ordered structure in the multilayer assembly, TE performance was enhanced significantly. The highest reported power factor of completely organic polymers, 2710 μW/(mK^2), was measured at room temperature.[15]

PANI is an intrinsically conducting polymer due to a conjugate π electron system in its structure.[83] However, the disordered molecule chains of PANI are two sides of one coin, because they impede carrier hopping, which results in low thermal conductivity but simultaneously low electrical conductivity. Therefore, the increased ordered regions in the molecular chain structure, which can be obtained by adding chemical solvents during the preparation of PANI, leads to the increment of carrier mobility and electrical conductivity.[84] Except for low conduction, the limitation of PANI as TE materials is that it can only be dissolved in rarely available solvents.[83] Therefore, in common cases, PANI has been used to combine with other organic or inorganic materials to form composites.

Apart from PANI, other conjugated polymers and small molecules have attracted much attention recently. Because the electron affinities of organic materials are usually low, n-type polymers are difficult to compound,[70] which can be solved with solution-processed self-doping perylene diimides (PDIs).[85] The mechanism for the n-type polymers with doping method is that the electrons are donated to the lower unoccupied orbital (LUMO).[86] The TE properties of PDIs were controlled and improved by tuning the side-chain length. Meanwhile, the effects of side-chain have also been studied with a series of self-doped π-conjugated polymer, cyclopenta-[2,1-*b*;3,4-*b* ´]-dithiophene-*alt*-4,7-(2,1,3-benzothiadiazole) (CPDT-*alt*-BT), with different counterions (Na^+, K^+, vs tetrabutylammonium) and lengths of alkyl chains.[87]

3.3. Graphene and composites

Recently, graphene has been proposed as one of candidates for lightweight, high-strength functional material owing to its superior electronic and mechanical properties (room temperature electron mobility of 15000 $cm^2\ V^{-1}\ s^{-1}$, specific strength of 130 GPa and stiffness of 1 TPa).[88] To date, easily scalable graphene-like materials in a form of separated flakes (exfoliated graphene, graphene oxide, and reduced graphene oxide) have been investigated for large-scale electronic devices.[89-91] Graphene has ascendant charge transport properties which can be utilized , but its thermoelectric efficiency is limited by the large thermal conductivity (up to 5000 W/(m K).[88] Thus, the thermoelectric figure of merit ZT of two-dimensional graphene sheet is low. Nanostructuring has been proven to be an effective strategy to reduce thermal conductivity by incorporating periodic holes in the crystal structure, which will increase phonon scattering without dramatically degrading

the electronic conductance.[92] In addition, substantial processes have also been reported to push forward its composite application, such as reduced graphene oxide (rGO) / PANI[93], rGO/PEDOT:PSS[94]. The strong p–p interaction between the graphene structure and aromatic rings of polymer conductors can facilitate electron delocalization and improve the electrical conductivity of the composites. Besides, the intrinsically low thermal conductivity of polymer will regulate the thermal conductance of graphene composite. Wang *et al* [95] reported a facile and green method for fabricating nanostructured rGO/PANI composites with highly enhanced thermoelectric properties. In this work, the refined PANI particles are homogeneously dispersed and orderly arranged on the rGO templates owing to the strong p–p conjugated interactions between PANI and rGO. The maximum electric conductivity and *ZT* of the rGO/PANI hybrid composites amazingly reached 1858.8S/m^{-1} and 4.23×10^{-4}, respectively. Moreover, Kim *et al*[64] introduced, for the first time, the highly conductive PEDOT:PSS/graphene composites fabricated by *in situ* polymerization and their applications in thermoelectric energy harvesting. In this *in situ* polymerization, PSS served as both a dispersant of rGO and a good dopant of PEDOT. The key advantage of this synthetic design is that PEDOT:PSS/graphene can be fabricated with rGO directly, without any further complex reduction since the conductivity of GO is poor. The electrical conductivity of the composites increased from 453 to 637 S/cm when the composite contained 3 wt.% of graphene, and the power factor ($S^2\cdot\sigma$) of the PEDOT:PSS/graphene composite was enhanced from 24.17 to 45.68 μW/(m K) due to the increased electrical conductivity.

3.4. Polymer TE composite materials

Incorporating nano-scaled inorganic materials into conducting polymer matrix is an effective method to enhance TE properties. Moreover, in contrast to rigid inorganic materials, this inorganic-polymer strategy facilitates facile synthesis and solution accessibility, which meets the printing requirements for the textile-based FTEGs fabrication. Up to date, two major groups of inorganic materials have been incorporated in a polymer matrix. Carbon nanotubes (CNTs) are widely recognized as one of the most effective fillers in polymer matrix.[96] Blended in a polymer matrix, CNTs are connected in series by Van der Waals force due to the presence of conductive polymers particles at the junctions, whose molecular vibrational spectra is mismatched with that of CNTs, thereby impeding the phonon transport at the connecting junctions. In contrast to this, these connecting junctions provide continues tunnels for electron transport without significant interruption, resulting in a high electric conductivity. This decoupling effect allows CNTs presenting a very high electrical conductivity and Seebeck coefficient when acting as fillers in the polymer, whilst the thermal conductivity remain relatively constant. Another category of inorganic materials, such as Bi, Te and Bi_2Te_3 nanostructures[97] are highly favourable for mixing with polymer matrix due to their high power factor at room temperature and solution processable. The fabrication of metal thermoelectric materials into thermoelectric modules involves high-temperature, long-term and high-cost processes.[98] Moreover, it is a grand challenge to integrate these rigid inorganic materials into FTEG which requires unusual topology for an enhanced practical efficiency. Synergetic combination of the easy processability of polymers and the excellent thermoelectric performance of inorganic semiconductors pave the way for the textile-based FTEGs fabrication. For instance, nano-sized carbon, that is, nanoparticles, nanotubes and

graphene, owns extraordinary electrical, thermal and mechanical properties, especially, extremely high electrical conductivity due to the great electron mobility. Furthermore, the π-π conjugated structure and large surface areas of carbon particles contribute to the contact between conducting polymers and these particles, which enhances electrical conductivity and Seebeck coefficient of polymers, because of the enhanced carrier mobility between the organic and inorganic materials. Additionally, thermal conductivity of these composites maintains comparable to that of organic polymers, because the bonding and vibration spectra between organic and inorganic materials are different. Therefore, TE properties of these composites are decoupled.[99] Inorganic TE materials incorporating into PEDOT: PSS and PANI are presented in this part, more detailed review of organic-inorganic composites can be found in the literature.[70, 100]

PEDOT:PSS has been filled with graphene[56], reduced graphene oxide (rGO),[64] expanded graphite[58, 59] or carbon nanotubes (CNTs),[60] to form TE composites. The electric conductivity of 60% CNT-filled PEDOT: PSS composites has been increased to 1350 S cm^{-1} which was higher than conventional Bi_2Te_3 semiconductors reported in Cho's group. In addition, Carbon-based materials have lower density (~1g/cm^3) in comparison to that of Bi_2Te_3 (~7.86 g/cm^3), which is especially important in lightweight textile-based energy conversion devices. EG post-treatment of PEDOT:PSS/CNTs nanocomposite films was reported to enhance electrical conductivity because of the removal of non-complexed PSS and the decrease of inter-bundle distance in the film.[60] Removing the insulating PSS not only enhanced electrical conductivity of PEDOT: PSS matrix but also decreased inter-CNT bundles, forming a continues electrical networks for the PEDOT:PSS/CNTs nanocomposites. Moreover, some metals were mixed into PEDOT:PSS, such as Au

nanoparticles,[61] tellurium nanorods.[62, 63], [101] Tellurium nanowires and PEDOT: PSS composite yields a higher *ZT* value than either one component.[62] This phenomenon contradicts the traditional believe that *ZT* value of a composite follows a law of mixture thus cannot surpass that of the individual constituents.[102] Although the mechanism of this phenomenon has been unclear to date, one of possible explanations is the interfacial change of the organic-inorganic composite.[103] Hetero junction charge transfer behaviour occurs when organic and inorganic materials combine, resulting in different carrier concentration and mobility at the interface between these materials.[104] Recently, Zaia *et al.* reported a maximum power factor of PEDOT: PSS/Te-$Cu_{1.75}Te$ alloy nanocomposite of 84 μW/(mK^2), which was increased by 22% than their former work.[24, 62] Recently, telluride-based nano-barbell structures coated with PEDOT: PSS was presented in Cho's group. These Te-Bi_2Te_3/ PEDOT: PSS is stable in water because of PEDOT: PSS surface coating, which allowing spray-printing fabrication of FTEGs.

Apart from common advantages of organic TE materials, PANI is much cheaper than other organic conducting polymers. Graphene,[105-109] rGO,[110] multi-walled carbon nanotube (MWNT),[111-114] single-walled carbon nanotube (SWNT)[72, 73, 115] have been hybridized with PANI and obtained improved TE properties. Particularly, PANI filling with graphene has attracted most attention, because graphene owns an enormous amount of π bridges which can form a great number of interfaces with PANI to improve carrier mobility and increase electrical conductivity. The first research of PANI/ graphene composite was reported in 2012, in which Seebeck coefficient, electrical conductivity and power factor was 41.3 μV/K, 8.63 S/cm, 1.47 μW/(mK^2), respectively.[105] Recently, a study showed that dispersing of graphene more homogeneously resulted in the improvement of Seebeck

coefficient to 26 μV/K.[106, 107] This is due to decreased aggregation, which is caused by strong Van de Waals attraction between the nanoplates; and increased number of graphene-PANI nano-interfaces in the composite. The electrical conductivity was also increased to 814 S/cm due to the reinforcement of π-π conjugation interactions between graphene and PANI by reducing impurities and structural defects in graphene. Therefore, the power factor was increased to 55 μW/(mK^2). Since CNTs/PANI composite was firstly investigated in 2010,[111] several groups have focused on the improvement of composite structure of CNTs and PANI. Instead of random distribution of CNTs, in parallel with the backbone of PANI was found to diminish defects of π-π conjugated interactions between interface surfaces and reduce carrier hopping barriers to increase carrier mobility. As a result, the electrical conductivity increased with little change of Seebeck coefficient.[114] Furthermore, Seebeck coeffecient increases due to the decrease of carrier concentration. The highest power factor reported so far was 220μW/(mK^2), which has been obtained from PANI/MWNT nanocomposite.[113]

3.5. Electric connectors

As mentioned above, in order to achieve high ZT values, thermoelectric materials should own high Seebeck coefficient, high electrical conductivity and low thermal conductivity. Recently researches have witnessed momentous progress in thermoelectric materials especially on heat transfer aspect.[116-118] In materials, substantial efforts have been made to reduce lattice thermal conductivity. For bulk materials, there are two strategies, alloying[119] and introducing phonon rattlers,[120] employed to scale down thermal conductivity. The notion of both alloying and phonon rattlers is introducing atomic disorder

either substitutionally or interstitially. Nano-structuring is another direction to improve ZT.[121] Although high ZT thermoelectric materials are developed, there are still many device-level challenges to apply thermoelectric materials into practical applications. Since ineffective dissipation of thermal energy jeopardize not exclusively the performance but also the life cycle and the reliability of devices. In electronic packaging, one should emphasize heat transfer aspect in thermoelectric modules and systems. Figure 2(a) is the schema of a typical FTEG unit. The n-type TE materials are coated on the surface of fiber/filament as TE legs. Instead of rigid electrodes, the interconnection is composed with flexible conductive fabrics. Although this structure satisfies the requirement of flexibility and deformability, the contact resistance issue is more significant in the FTEGs than that in the traditional rigid TEGs. As shown in Figure2 (b), if the interconnection layer is fabricated with single-layer multifilament yarn, the porous region with air insulation pockets exist between TE material and the connecting fabric. The electrical conductivity will change as the result of the change of number of contact points between the single-layer yarn and the TE leg when the FTEG is deformed. Actually, the interconnection layer is usually composed of multifilament yarn with several layers (Figure 2(c)).[2] In such a case, the electrical conduction and thermal conduction have a profound effect on the device performance.[122] The thermal and electrical conductivity of micro-gaps, such as air, is typically much lower than that of TE materials and interconnection fabric. Therefore, the conduction of heat flux in non-conducting regions is smaller than the entire nominal contact areas, leading to increased interfacial thermal resistance.[123] A similar effect is expected for electric conductivity at the contact region. The figure of merit of this FTEG module (ZT_{mod}) can be calculated with the following equations:

$$ZT_{\mathrm{mod}} = \frac{S^2 T}{K_{\mathrm{mod}} R_{\mathrm{mod}}} \quad (6)$$

$$K_{\mathrm{mod}} = \frac{2\kappa_n A_n}{l} + K_c \quad (7)$$

$$R_{\mathrm{mod}} = R_{legs} + R_c = \frac{\rho_n l}{2A_n} + R_c \quad (8)$$

where A and l represent the cross-sectional area and length of the TE material, respectively; ρ is the specific electric resistance; K_{mod} and R_{mod} are the thermal conductance and electric resistance of the module, respectively; K_c is the thermal contact conductance; R_{legs} and R_c are the resistance of TE legs and the contact resistance, respectively.

In addition to outer thermal contact resistance, thermal expansion and electrode issues should be highly concerned. Traditionally, thermoelectric systems often consist of three different parts, thermoelectric elements, interconnectors, and packaging enclosures. In electronic packaging, apart from thermoelectric elements fabrication, interconnector preparation is also play an essential role in device performance. In terms of thermal transfer, if the fabrication materials possess different thermal expansion coefficients, it will cause the degradation of the contacts between thermoelectric elements and interconnector, resulting in poor performance or even failure of the device.[124] Moreover, the leakage or degraded contact of electrode and thermoelectric pellet will induce electrical contact resistance as well.[125] As for electrode, materials of electrode applied in thermoelectric generator are usually metal which are in high electric conductivity. These metal atoms tend to diffuse into thermoelectric materials at high temperature, thus leading to the impurity of thermoelectric materials and changing the carrier density, even the type of carrier. In order to avert diffusion issue, diffusion barrier should be used as an intermedium between

electrode and thermoelectric pellet. There are a few metals used to form diffusion barriers for specific applications, such as nickel,[126] nichrome, zirconium, vanadium, and tungsten, ect. Conductive ceramics, such as tantalum nitride, indium oxide, copper silicide, are another kind of materials employed for the same specific objectives. In Cheng's group,[127] TaN diffusion barrier for n-type antimony telluride (SbTe) has been developed. This TaN barrier has strong ionic Ta–N bonding, exhibiting high-temperature thermal stability. Moreover, a high total energy of 4.7 eV/atom for the TaN/Sb_2Te_3 system indicates that TaN could effectively suppress the formation of SbTe-compounds interfacial layer. Thus, a well-designed contact is required to have a high diffusion barrier and a low electrical/ thermal contact resistance.

4. Structures of FTEG Devices

Generally, structure of most FTEG devices to date can be divided into two categories, two-dimensional fabric form (2D) and one-dimensional fiber/yarn form (1D), although various new materials are continuously emerging. Embedding rigid elements into flexible substrates to form devices in 2D structure is a prevalent method. But FTEG devices made by this method can cause uncomfortable experience if the TE devices are in direct contact with human skin. 1D FTEGs, in such forms as yarns and fibers, have attracted researchers' attention, because they have the enormous potentials to form higher dimensional structures in various configurations directly.

4.1. Two-dimensional (2D) structures

Normally, ultra-thin films of glass, thin films of polyimide (also termed Kapton) and PVDF *etc.* are used as substrates to ensure the flexibility. For some applications, high temperature resistance is essential to endure stability in fabrication and usage. Thermal energy is usually harvested by the films in the in-plate direction for little limitation of maximum thickness, as illustrated by Figure 3. The heat flow direction is along the thickness direction of the curved film.

The disadvantages of the curved film-based TE generators are lack of air-permeability, poor in three dimensional deformability, low damage tolerance although they are stretchable and bendable in one direction. Therefore, fiber-based structures of TE devices are designed, for example, inorganic FTEGs are embedded into fabrics, or textiles are fabricated with conductive materials coated wires. In the FTEGs, individual elements are connected with mental wires and are embedded and infiltrated in flexible fabric substrate. This structure combines advantages of TE materials (e.g. great TE properties) and textiles (e.g. flexibility). Recently, an FTEG integrated with Bi_2Te_3 and Sb_2Te_3 as TE elements on a woven fabric made from glass fibers has been fabricated by using screen-printing technique.[18] This TE devices had excellent flexibility, because its normalized resistance in two perpendicular directions was stable when it was bent with 20mm radius or 120 cycles of repeated bending with 50mm radius. The output power was 3.8 W/cm^2 with 8 thermocouples of Bi_2Te_3 and Sb_2Te_3 elements, when the temperature difference was 50 K. Kim *et al* made a FTEG from a combination of polymer-based fabric and 12 thermocouples which consisted of $Bi_{0.5}Sb_{1.5}Te_3$ and $Bi_2Se_{0.3}Te_{2.7}$, by using the dispenser printing method.[128] When the temperature difference was 15K, the power of the FTEGs was 224

nW. The generated power was 146.8 nW when a fabric of shirt with the FTEGs was worn by a human subject at ambient temperature of 5℃. Lu *et al* showed a FTEG with nanostructured Bi_2Te_3 and Sb_2Te_3 depositing on a silk fabric.[129] When temperature difference was 35 K, the maximum output power of the FTEGs with 12 thermocouples was much lower than the other work, approximately 15 nW. The embedded-structure has some disadvantages, for example, the comfort is sacrificed due to the hardness and impermeability of the embedded FTEGs.

Instead of the embedded-structure, a knitted fabric panel was firstly fabricated by alumel and chromel wires around glass-epoxy substrates in 2002, as shown in Figure 4.[17] These metal wires interconnected and formed thermocouples. The maximum output power was 0.166 μW per couple at a temperature difference of 26 K. Recently, the thermoelectric knitted and woven textiles were directly fabricated with sheath-core structure flexible yarns, whose cores were polyacrylonitrile (PAN) nanofibers and n- and p-type semiconductor sheaths were Bi_2Te_3 and Sb_2Te_3, respectively.[20] When the temperature difference was 200℃, the output power in the textile thickness direction was 8.56 W/m^2. The direct fabrication with 1D FTEGs provides great promises for the development and application of flexible FTEGs. Further efforts should be made in the future to improve the TE performance and realize the application in heat condition. Another example of FTEG fabrics was a polyester fabric coated with 5 wt% DMSO-mixed PEDOT: PSS was cut into strips which were sewed on uncoated fabric and linked with conductive connection.[130] The output voltage of this FTEG fabric with 5 strips was 4.3 mV at a temperature difference of 75.2 K.

4.2. One-dimensional (1D) structures

1D FTEGs are based on yarns, filaments or fibers, which have attracted some research attention, due to their flexibility and fabrication possibility in textiles. For example, Nickel and silver were deposited as adjacent strips on silicon fiber.[19] The Seebeck coefficient of this 1D FTEGs was approximately 19.6 μV/K. Yarns with a similar structure were fabricated with Bi_2Te_3 (n-type) and Sb_2Te_3 (p-type) depositing on PAN nanofibers, whose Seebeck coefficients were -176 and 178 μV/K, respectively.[20] This adjacent coating 1D structure maintained flexibility in bending and twisting, and simultaneously formed p- and n-type junctions who owned better TE properties than single p- or n-type leg, which can be used to fabricate 2D TE devices directly.

Coated glass fibers with 300 nm PbTe nanocrystals in thickness[131] exhibited excellent TE properties and flexibility, whose electrical conductivity, Seebeck coefficient, thermal conductivity, power factor, ZT at 400 K and a bending curvature was 172.4 S/m, 350 μV/K, 0.226 W/(mK), 0.41 mW/(mK^2), 0.72, and 84.5°, respectively. Recently, the same group reported an intensively research about Ag2Te nanocrystals-coated nylon fiber mesh at annealing temperature of just above 150 ℃, solving the problem that high temperature (300~350 ℃) annealing process. The FTEG device, which was composed with p-type PEDOT: PSS coated nylon and n-type air plasma treated Ag_2Te nanocrystals-coated nylon, showed output power of 5 nW at temperature difference of 20 K, with calculated Seebeck coefficient of 187 μV/K.[132]

Although 1D FTEGs offers more opportunities to fabricate higher dimensional structure, the effects and theoretic limitation lack investigation, if 1D FTEGs are assembled together. For example, if yarns are composed with TE fibers, the interaction between fibers may influence TE performance. Additionally, structure of 1D materials, such as the cross-section shape or diameter, may have some effects.

4.3. Influences of structure parameters on FTEGs performance

Except for considering the dimension effects on the performance of FTEGs, the cross-sectional area and length of p- and n-type junctions and the space distance between them demand to be contemplated seriously. In the FTEGs, heat energy can be transformed into electrical energy with p- and n-type junctions as conductors. Meanwhile, in the FTEGs, heat loss caused by radiation and convective heat transfer happens simultaneously, which degrades the performance of FTEGs dramatically. Many researchers studied rigid TEGs and pointed out that radiation and internal natural convection was proportional to the surface area and temperature of objects.[133-136] However, although the important effects of porous media on heat transfer have been pointed out since late 1990s,[137] few works have been done for analysing parasite heat loss in FTEGs. Especially, fiber-based FTEGs are usually fabricated with porous materials.

Moreover, if the TE elements formed on fabrics, heat convection of FTEGs will be affected by the textile structure. The influence of textile material parameters, such as fiber diameter, pore size, porosity, bulk density and thickness, on natural convection and radiative have been studied intensively.[138-145] The result of convective heat transfer is the decrease of

thermal resistance and the increase of thermal conductivity.[146] However, to our knowledge, no research about the influence of these parameters on FTEGs has been done.

5. Fabrication Methods

Fabrication methods have great effects on TE properties and stability of resultant devices. In this section, several fabrication methods, reported in the literature, are summarized and compared, the challenges are discussed.

Fabrication methods can be classified into two categories: surface modification and embedding. Surface modification is that TE materials deposit on commercial fibers, yarns or fabrics as substrates, which can ensure the flexibility of FTEG devices. If the substrates are fibers or yarns, they can be used to fabricate complex configuration FTEG devices, especially the fabrics can be woven or knitted with them. Therefore, the advantages of woven or knitted fabrics will exhibit in the FTEG devices, such as flexibility, stretch-ability and gas permeability. In contrast, embedding method sacrifices some flexibility and comfort, because the p- or n-type junctions made of rigid TE materials are usually penetrated into commercial fabrics.

To fabricate FTEG devices by surface modification, the techniques include drop-casting, [24, 60, 63, 71, 77, 84, 105-107, 109, 113, 147] dip coating,[74, 130-132] spin coating,[79-81, 148] radio-frequency (RF) magnetron sputtering,[20, 149, 150] thermal vapour deposition,[19, 151-153] screen printing [18, 154] and dispenser printing. [128] Drop-casting is one of the most common techniques due to the easy operation without vacuum or high temperature condition. The prepared

inks/solution is deposit onto the surface of a flexible substrate. However, in literature, most used substrates are films instead of fibers, yarns or fabrics. Therefore, this method is yet to be explored for textile industry. In contrast, dip coating can be used on the surface of fibers and fabrics directly, which is that the substrates are immersed into particular solutions. Spin coating is that the prepared solution is dropped on flat substrates with a high rotational speed. RF magnetron sputtering is that elements of TE compounds are sputtering directly on substrates, with different RF power to control exact stoichiometric ratio of compounds. But this technique must be operated under a pressure of $10^{-4} \sim 10^{-5}$ Pa, which is expensive and has to use batch production. Compared with RF magnetron sputtering, although TE films can be fabricated with thermal vapour deposition technique, the operation condition of this technique is not only under a very low pressure, but also at high temperature (150~300℃) for inorganic TE materials deposition. Screen printing and disperse printing are the most desirable methods for fabric substrates.

Recently, an increasingly number of FTEGs fabricated by screen printing strategy have been reported. Cho's group has developed several lightweight, FTEGs via screen printing.[155] Wearable fabric based FTEGs is one typical design of these devices, which was printed with synthesized liquid-like pastes of n-type (Bi_2Te_3) and p-type (Sb_2Te_3) TE materials onto a glass fabric for the FTEGs by employing screen printing technique. The synthesized pastes permeated through the meshes of the fabric and formed films of TE materials in a range of thickness of several hundreds of microns. This technology integrated inorganic-based TE materials to textile-based substrate successfully, presenting an efficient way of fabricating an extremely flexible, light, and high-performance FTEG. Lately, Cho's group proposed a FTEG which was fabricated on a SiO_2/a-Si/quartz substrate via the screen

printing process, and then separated the rigid quartz substrate from the original FTEG by laser multi-scanning lift-off process.[156] This freestanding FTEG was low packing density and foldable. In this light, the substrate variety option of screen printing allows synthetical fabrication for the FTEGs.

Apart from distinctive operation conditions are required for the above mentioned fabrication methods, in order to obtain better TE properties of the most common materials like Bi_2Te_3 and Sb_2Te_3, annealing at high temperature (100~530℃) is another potential challenge, because of the increase of cost and limitation to sorts of substrate materials which can endure the temperature.

6. Performance Characterization

As TE energy conversion efficiency and power factor of materials can be expressed and calculated as Equations (1) and (3), respectively, the characterization of electrical conductivity, Seebeck coefficient and thermal conductivity is very critical and important. However, to obtain exact values of these parameters presents a challenge due to heat flows which should maintain a time-invariant steady state during the measurement process. Besides, the secondary parasitic heat flows, which are difficult to control, can result in a significant error, except for usual electronics errors.[157] To date, instruments have been used for measuring the TE properties are usually home-made without uniform standards. Therefore, this part focuses on the principles of these characterization.

6.1. Electrical conductivity

The commonly used measurement method of electrical conductivity (σ) is a four-point probe method or a van der Pauw's method. Figure 5(a) illustrates schema of the four-point probe method. Four probes are contacting with the TE material. If a current, I, flows from probe A to D, a voltage, V, will be measured between probe B and C.[158] The electrical conductivity can be calculated by:

$$\sigma = \frac{\ln 2}{\pi t}\frac{I}{V} f \qquad (9)$$

where t is the thickness of the sample, f is a correction factor.

The four-point probe method is based on the assumptions that the thickness of the sample is uniform and the surface does not have isolated holes.[159] Therefore, the preparation process should make the sample satisfy these assumptions. Besides, the four probes are at the same temperature. Otherwise, if the input current is DC, temperature gradient will generate, as the result of the Peltier effect. And a Seebeck voltage should be considered during the calculation.[160] Therefore, AC or current with periodically changing direction should be used in the measurement to eliminate the corresponding Seebeck voltage.

The van der Pauw's method, which was presented in late 1950s,[159, 161] can be used to measure the specific resistivity of materials in arbitrary shape. This method is an effective way to eliminate contact resistances which are generated during the measurement and have a significant influence on the measuring results.[162] In contrast to the four-point method, the contacts in van der Pauw's method are at the circumference of the sample, instead of being placed along a line on the sample surface, as shown in Figure 5(b).

6.2. Thermal conductivity

Thermal conductivity (κ) is an important physical parameter for TE materials and devices. The measurement methods of thermal conductivity can be divided into two categories: a steady-state technique and a dynamic-state technique. Figure 6 illustrates the principle of a steady-state technique, which is commonly used to measure thermal conductivity of bulk materials. Then, the thermal conductivity, κ , can be expressed as follows:

$$\kappa = \frac{QL}{A\Delta T} \qquad (10)$$

where Q is the heat supplied to the source; L is the distance between thermometers; A is the cross-section area of the sample; ΔT is the temperature difference between thermometers, $\Delta T = T_1 - T_2$. This method is based on the assumption that the cross-section of the sample is uniform and that any form of heat losses is negligible.[163] Therefore, it is important to choose wires to connect the sample and thermometers and to operate the measurement at good vacuum condition. Besides, the length of sample has a dual effect: for a long sample, the measurement errors are minimized, while the lateral heat losses increase.[160] Therefore, the sample with low thermal conductivity owns usually short length. For fabrics, Kawabata Evaluation System for Fabrics (KESF by Kato Co Ltd) has been used extensively for measurement of thermal conductivity in textile industry.

Compared with the steady-state technique whose heat losses must be measured exactly, the dynamic-state technique is preferred due to the elimination of infrared irradiation. Laser

flash method and 3ω method are two common ways of the dynamic-state technique for measuring thermal conductivity. Figure 7 illustrates the most important parts of a laser flash instrument. One surface of the sample is exposed to the laser light no more than a millisecond. If the temperature of another surface of the sample is monitored with an IR detection, one peak temperature, caused by the complete heat loss from the sample, will be obtained. The fundamental thought is to obtain thermal conductivity by measuring thermal diffusivity, λ, according to the following:

$$\lambda = \frac{\kappa}{c_V} \tag{11}$$

where c_V is the specific heat per unit volume. The thermal diffusivity is measured with the laser flash method:

$$\lambda = \frac{1.37 d^2}{\pi^2 t_{1/2}} \tag{12}$$

where d is the thickness of the sample; $t_{1/2}$ is time when the temperature of the sample surface without suffering laser light reaches one-half of the peak temperature. The detection should fulfil relative strict boundary conditions to reduce errors: the sample surface can evenly absorb the laser energy; the disappearance time of heat pulse can be neglected; the measurement time should be short enough for avoiding heat losses from the sample.[163]

3ω method was firstly used to measure thermal conductivity of amorphous solids in 1987, [164] which soon extended to the measurement of thin films.[165] Nowadays, this method is widely used to measure thermal conductivity of TE films and coatings in dynamic state. Figure 8 shows the measurement set-up in this method. A metal strip is deposited onto the film surface, which simultaneously plays two roles: a heater and a thermometer. An AC current with frequency ω flows in the metal strip and generates a temperature wave with frequency 2ω. The wavelength or the penetration depth ($\frac{1}{q}$) is given by

$$\frac{1}{q} = \left(\frac{\lambda}{2\omega}\right)^{1/2} \quad (13)$$

After measuring value of thermal diffusivity (λ), thermal conductivity (κ) can be obtained according to Equation (8).

For FTEGs, alternative measurement of thermal conductivity can be made by a commercial instrument, Thermolab unit in Kawabata Evaluation System of Fabrics (KESF^{TM}) system by Kato Instruments.

6.3. Seebeck coefficient

The definition of Seebeck coefficient is

$$S = \lim_{\Delta T \to 0} \frac{\Delta V}{\Delta T} \quad (14)$$

where ΔV represents the open-circuit potential difference; ΔT is the temperature difference. Two common measurement methods are operated: the first is that the measurement points of thermocouples (Points A and B in Figure 9(a)) contact with a sample directly; the other is that these points are placed at the heater and heat sink as depicted in Figure 8(b). As shown in Figure 8(a), if the thermocouples have a temperature different from that of the sample, which can cause a temperature gradient in the thermocouples, the measured temperature will deviate from the real value at the contact regions from where the electric potential will generate. The second method neglects the temperature difference between the sample ends and heater/sink at the interface.[160] For FTEGs, the Seebeck voltage is tested by a lab-made set-up which normally consists of heating and cooling device with feedback control, digital multimeter and digital thermometer. The running water keeps the cold side temperature. The hot side temperature is controlled by the electric power source regulator with temperature feedback. Figure 10 illustrates heat transfer detail between the hot side contact layer and FTEG. Heat transfer will take place on the surface of each material when there is a temperature difference. Actually, upon closer inspection, the contacting surfaces of fibrous materials are somewhat roughness or non-conforming, making the real contact area is smaller than the corresponding contact area. Thus, the surface roughness introduces air gaps between contacting materials, resulting porous insulation. The thermal conductivity of micro-gaps, such as air, is typically much lower than that of common solid materials. Therefore, the conduction of heat flux in non-conducting regions is smaller than the entire contact areas, leading to increased interfacial thermal resistance. In our measurement, all mechanical interfaces are sealed with thermal compound to reduce heat loss. Once the device reaches

steady state with a constant temperature gradient, the Seebeck voltage of the FTEG is measured using a digital multimeter (Keithley 2700). The temperature gradient across the sample is tested by digital thermometer (Anbat AT4516) with dual K input. All tests are processed at room temperature.

6.4. Figure-of-merit

According to Equation (1), although the value of figure-of-merit (ZT) can be obtained by measuring Seebeck coefficient (S), thermal conductivity (κ) and electrical conductivity (σ) separately, it was firstly presented with a single instrument based on the Peltier effect by Harman in the end of 1950s.[166, 167] Therefore, ZT can be obtained directly from the ratio of potentials in the adiabatic and isothermal condition. The detailed deduce can be found in the work by Harman.[166] The expression of ZT is:

$$ZT = \frac{S^2 \sigma T}{\kappa} = \frac{V_T}{V_i} - 1 \qquad (15)$$

where V_T is the adiabatic potential, V_i is the isothermal potential.

Although this method can be applied to the measurement of rigid TEGs, it has some potential drawbacks for being applied to FTEGs. It is the result of a great deal of uncertainty in Seebeck coefficient and electrical conductivity which are caused by the large

intrinsic resistance of polymer. Besides, the contacts on flexible substrates are not so good as those on rigid ones, which can increase the measurement errors.

7. Potential Applications and Benchmarks

Based on the Peltier effect and Seebeck effect, the potential application areas of flexible TE devices fall into two categories: FTE coolers (FTECs) converting electric into heat energy, and FTEGs converting heat into electric energy. In the cooling area, FTECs parasitize in mobile refrigerators, electronic devices, air-conditioning systems, buildings etc., exhibiting their advantages like small volume and exact temperature control without vibration or noise. Although majority of devices are rigid, they have been applied to substitute traditional cooling system, installing in refrigerators and electronic devices like central processing unit.[168-170] Additionally, the coolers combined with heating system can utilize the solar energy to cool and warm rooms in summer and winter, respectively.[171] A thorough and systematic review on rigid TE cooling can be referred in the literature.[172] Besides, substantial energy saving with personal micro-climate control method is an effective and promising way to deal with the environmental pollution and climate change issues caused by the current air-conditioning methods.[173] This target can be achieved with FTECs whose flexibility and light weight overcome the drawbacks of traditional TECs.[174] When the surrounding temperature is higher than the average skin temperature, cloth system with FTECs can keep the micro-climate cool. Thus, such clothes are especially useful to prevent heat-stroke for people who work under high temperature conditions, such as building labourers in subtropic and tropic regions, as well as steelworkers and so on.

The first practical application in the world, SNAP-3B (Systems for Nuclear Auxiliary Power) radioisotope TEG in a launched U.S. spacecraft, can be traced back to the early 1960s.[175, 176] After that, the application of radioisotope TEGs was gradually expanded to terrestrial areas like weather stations, navigational aids, subsea operations, etc..[177] Although photovoltaic cells can capture solar energy, solar TEG is another potential key method to convert it into electric power, which can be used to deep-space probe missions in near sun obits and some terrestrial applications.[178] These applications of rigid TEGs encourage the research on FTEGs, because of the typical advantages of the later one. And the potential application areas of FTEGs are extremely large: from space and military to automobile and airplane to biomedicine to smart textiles and so on, utilizing miscellaneous heat sources like waste heat from transportation tools and bio-therm. For example, when astronauts engage in an extravehicular activity, they wear hermetical space suits in outer space condition with temperature range being -233 ℃~121 ℃.[179] The traditional space suit control thermal condition is liquid cooling and ventilation garment. The drawback of this garment is bad air permeability, which is the result of the ventilation unit or airflow duct over the garment.[180] Therefore, The combination of FTECs and FTEGs takes their advantages to provide a potential solution for dealing with the thermal and moisture comfort issue of the present space suits. When the outer space temperature is higher than body temperature, FTEGs will provide electrical energy and support the operation of FTECs. Thus, the micro-climate temperature of astronauts will be controlled without any liquid cooling system. Besides, during recent years, the major auto magnates, including Volkswagen, BMW, Ford, Toyota, Honda, Nissan and GM, have launched projects about waste heat recovery with TEGs.[181] In a common vehicle, more than two-thirds energy

offered by gasoline-fuel wastes as waste heat discharged by exhaust gas and cooling system, which is approximate tens of kilowatts of heat losses.[10, 176, 182] Therefore, TEGs can be fixed on the surface of related parts like the exhaust pipe and radiator in vehicles to convert the waste heat into electricity.[171] A challenge for the utilization of FTEGs on exhaust pipe is the polymer stability, because the temperature of exhaust gas in vehicle is as high as 500 ℃.[176] Thus, the selection of suitable materials for FTEGs using on exhaust pipe is extremely important. But the temperature of a radiator is only approximate 100 ℃, which is quite appropriate for the operation of FTEGs. Taking advantage of the flexibility, textile-based TEGs can match the pipe or radiator perfectly, even if the contours are irregular. Hence the large amount of energy dissipated as waste heat can be converted to electrical energy with FTEGs.[183]

Moreover, one of most important applications of textile-based FTEGs is to convert human body heat into electrical energy. As a kind of low-quality energy, human body heat is normally thermostat at approximate 37℃, which is generated with metabolic process.[184] The most obvious advantages of this energy are that it is released 24 hours a day and 7 days a week with little relation to movement of human and can be collected from the whole surface of human body. Therefore, by the conversion, textile-based FTEGs can be used to support the operation of miniature electronic devices, such as sensors[185, 186] and implantable medical devices (IMD) that includes cochlear, drug pump, neuro-stimulator, muscle stimulator and pacemaker. These devices require from only several microwatt to milliwatt to keep their operation.[187, 188] Since the first IMD, a pacemaker, was presented in 1972, which was powered with batteries, IMD have been widely used to diagnosis, prognosis and treatment.[189] One of challenges for the development of IMD relies on that

its batteries, the energy source of the device, will be over lifespan after long-time usage.[190] A stable and immortal power to maintain the function of IMD is required, which can reduce unnecessary surgery and save money for patients. Therefore, a potential method for solving the problem is that FTEGs power IMD.

Since the first market-oriented rigid generator devices was fabricated and equipped on a wristwatch in 1999,[15] the topics have been studied by several groups and the performance of their devices may provide benchmark for future development of FTEGs. A wireless sensor node was powered by a human body heat with a watch-size rigid generator device ($3\times3\times1\,cm^3$).[184, 191] In the device, p- and n- type nodes were integrated as a thermocouple. Thousands of thermocouples composed a thermopile which was etched into substrate to form a rim. The rim structure was designed to prevent the decrement of parasitic heat in traditional sandwich structure with thermopiles placed between a hot plate and a cold plate.[192] The output voltage of a device reached 53mV/ ($K\cdot cm^2$) in 2007,[193] that of a late one was increased to 12.5 V/ ($K\cdot cm^2$) in 2009 [194, 195] with the open-circuit output voltage of 0.15V in office condition. In term of area, a 9 cm^2 rigid TEG device generated 20 μW at 22℃, that is, a 2.2 $\mu W/cm^2$ power density.[196] In term of mass, 330 μW/g was reported from a rigid TEG with heat sink working at 22.6±0.4 ℃ with 0.9 m/s air flow.[197]

8. Conclusion

In this paper, an overview and review on the state-of-arts of FTEGs has been presented in the following aspects: the operational mechanism, materials, device structures, fabrication

methods, characterization and applications. Inorganic TE materials have attracted great attention due to their outstanding TE performance, although they are rigid, fragile and require high processing temperature. Conducting polymers like PEDOT and PANI are flexible and processed at low or room temperature via solution routs, whose TE properties have been improved consistently. The structures of reported FTEG devices are summarized and compared. Two types of fabrication methods are covered: surface modification and embedding approaches. FTEGs have great potentials to provide power wearable electronic devices and energy harvesting from heated machines like engines.

Although FTEGs exhibit enormous potentials in applications, very few work have been published indicating the early stage of development in FTEGs. What are the limitations that impede their development and utilization in reality? What should be do in order to push forward? The answers are multiple folds. First, the performance and stability of TE materials for FTEGs should be improved significantly. Inorganic TE materials face the challenge of flexibility, without sacrifice of their superior TE properties. The performance of conductive polymers is greatly inferior to that of inorganic materials. Because little is known on the environmental stability of conductive coating layer on fibers and textile fabrics in FTEGs, the reliability of the devices is doubtable. Secondly, although embedding structure can offer flexibility to some extent, the hard and brittle devices may cause unpleasant and uncomfortable when the device contacts with human skin surface. Fiber-based FTEGs are much desired. Very little has been reported on the structural design and analysis of FTEGs based on solid scientific foundation, for which more research is required. Considerations should be directed to the effects of molecular orientation and clustering, reduction of hopping barrier and contact resistance as well as textile structural design. At

present, the measurement techniques are not unified. For instance, instruments for thermal conductivity, Seebeck coefficient and electrical conductivity are home-made in most cases. Furthermore, the current fabrication methods are only limited in laboratory, which are difficult to realize mass production either in batch or continuous production. The fabrication methods to integrate these TE materials into the FTEGs should be further explored. In addition, the conversion efficiency of FTEGs is still relatively low, especially considering the low temperature difference in wearable applications. Finally the current cost–benefit ratio is high hindering the applications. For example, the cost of rigid TEG system was ~US$30/watt in 2014, which should be as low as ~$5/watt to satisfy the economical transportability.[183]

Acknowledgements
The work has been partially supported by Research Grants Council of Hong Kong SAR Government, China (Grant No. 15204715) and The Area of Excellence Fund, Hong Kong Polytechnic University (Grant No.1-AAB3). Zhang acknowledges a postgraduate scholarship from the Hong Kong Polytechnic University.

References

[1] B. Yang, W. Zeng, Z.H. Peng, S.R. Liu, K. Chen, X.M. Tao, *Adv. Energy Mater.* **2016**, *6*.

[2] S. Chen, X.M. Tao, W. Zeng, B. Yang, S. Shang, *Adv. Energy Mater.*, 10.1002/aenm.201601569

[3] W. Zeng, X.M. Tao, S. Chen, S. Shang, H.L.W. Chan, S.H. Choy, *Energy Environ. Sci.* **2013**, *6*, 2631.

[4] J. Zhao, G. Wu, Y. Hu, Y. Liu, X.M. Tao, W. Chen, *J. Mater. Chem. A.* **2015**, *3*, 24333.

[5] J. Sun, Y. Huang, C. Fu, Y. Huang, M. Zhu, X.M. Tao, C. Zhi, H. Hu, *J. Mater. Chem. A.* **2016**, *4*, 14877.

[6] X.M. Tao, *Handbook of Smart Textiles*, Springer Singapore 2015.

[7] L.I. Anatychuk, R.R. Kobylianskyi, *Mater. Today Proc.* **2015**, *2*, 849.

[8] L.R. Liang, C.Y. Gao, G.M. Chen, C.Y. Guo, *J. Mater. Chem. C.* **2016**, *4*, 526.

[9] W. He, S.X. Wang, C. Lu, X. Zhang, Y.Z. Li, *Appl. Energy.* **2016**, *162*, 1251.

[10] Y.Y. Hsiao, W.C. Chang, S.L. Chen, *Energy.* **2010**, *35*, 1447.

[11] L.E. Bell, *Science.* **2008**, *321*, 1457.

[12] X. Liu, Y.D. Deng, Z. Li, C.Q. Su, *Energy Convers. Manage.* **2015**, *90*, 121.

[13] W. Zeng, L. Shu, Q. Li, S. Chen, F. Wang, X.M. Tao, *Adv. Mater.* **2014**, *26*, 5310.

[14] Y. Yang, G.D. Xu, J. Liu, *J. Med. Devices.* **2014**, *8*, 014507.

[15] M. Kishi, H. Nemoto, T. Hamao, M. Yamamoto, S. Sudou, M. Mandai, S. Yamamoto, 18th International Conference on Thermoelectrics, 1999

[16] S. Lv, W. He, L.P. Wang, G.Q. Li, J. Ji, H.B. Chen, G. Zhang, *Appl. Therm. Eng.* **2016**, *109*, 138.

[17] N. Yamamoto, H. Takai, *Electr. Eng. JPN.* **2002**, *140*, 16.

[18] S.J. Kim, J.H. We, B.J. Cho, *Energy Environ. Sci.* **2014**, *7*, 1959.

[19] A. Yadav, K.P. Pipe, M. Shtein, *J. Power Sources.* **2008**, *175*, 909.

[20] J.A. Lee, A.E. Aliev, J.S. Bykova, M.J. de Andrade, D. Kim, H.J. Sim, X. Lepro, A.A. Zakhidov, J.B. Lee, G.M. Spinks, S. Roth, S.J. Kim, R.H. Baughman, *Adv. Mater.* **2016**, *28*, 5038.

[21] H.J. Goldsmid, *Proceedings of the Physical Society of London Section B.* **1956**, *69*, 203.

[22] J.W. Zhou, B.L. Liao, G. Chen, *Semicond. Sci. Technol.* **2016**, *31*.

[23] A.F. Ioffe, *Semiconductor Thermoelements and Thermoelectric Cooling*, Infosearch, London, 1957.

[24] E.W. Zaia, A. Sahu, P. Zhou, M.P. Gordon, J.D. Forster, S. Aloni, Y.S. Liu, J.H. Guo, J.J. Urban, *Nano Lett.* **2016**, *16*, 3352.

[25] C. Wood, *Rep. Prog. Phys.* **1988**, *51*, 459.

[26] S. Lee, G. Chen, *Innovative Thermoelectric Materials: Polymer, Nanostructure and Composite Thermoelectrics*, Imperial College Press **2016**.

[27] A.T. Burkov, M.V. Vedernikov, *CRC handbook of thermoelectrics* D.M. Rowe (Ed.), CRC Press **1995**.

[28] S. Walia, S. Balendhran, H. Nili, S. Zhuiykov, G. Rosengarten, Q.H. Wang, M. Bhaskaran, S. Sriram, M.S. Strano, K. Kalantar-zadeh, *Prog. Mater. Sci.* **2013**, *58*, 1443.

[29] J. He, Y. Liu, R. Funahashi, *J. Mater. Res.* **2011**, *26*, 1762.

[30] C. Han, Q. Sun, Z. Li, S.X. Dou, *Adv. Energy Mater.* **2016**, *6*.

[31] M.R. Gao, Y.F. Xu, J. Jiang, S.H. Yu, *Chem. Soc. Rev.* **2013**, *42*, 2986.

[32] J.F. Li, W.S. Liu, L.D. Zhao, M. Zhou, *NPG Asia Mater.* **2010**, *2*, 152.

[33] T.O. Poehler, H.E. Katz, *Innovative Thermoelectric Materials: Polymer, Nanostructure and Composite Thermoelectrics*, Imperial College Press **2016**.

[34] L. Ainsworth, *Proceedings of the Physical Society of London Section B.* **1956**, *69*, 606.

[35] H.J. Goldsmid, *Proceedings of the Physical Society of London.* **1958**, *71*, 633.

[36] B. Poudel, Q. Hao, Y. Ma, Y. Lan, A. Minnich, B. Yu, X. Yan, D. Wang, A. Muto, D. Vashaee, X. Chen, J. Liu, M.S. Dresselhaus, G. Chen, Z. Ren, *Science.* **2008**, *320*, 634.

[37] S. Il Kim, K.H. Lee, H.A. Mun, H.S. Kim, S.W. Hwang, J.W. Roh, D.J. Yang, W.H. Shin, X.S. Li, Y.H. Lee, G.J. Snyder, S.W. Kim, *Science.* **2015**, *348*, 109.

[38] B.L. Huang, M. Kaviany, *Phys. Rev. B.* **2008**, *77*.

[39] G.S. Nolas, D.T. Morelli, T.M. Tritt, *Annu. Rev. Mater. Sci.* **1999**, *29*, 89.

[40] G.A. Slack, *CRC handbook of thermoelectrics*, CRC Press 1995.

[41] R.Q. Guo, X.J. Wang, B.L. Huang, *Sci. Rep.* **2015**, *5*.

[42] A.J. Gross, G.S. Hwang, B.L. Huang, H.X. Yang, N. Ghafouri, H. Kim, R.L. Peterson, C. Uher, M. Kaviany, K. Najafi, *J. Microelectromech. Syst.* **2011**, *20*, 1201.

[43] T. Graf, C. Felser, S.S.P. Parkin, *Prog. Solid State Chem.* **2011**, *39*, 1.

[44] L.H. Huang, Q.Y. Zhang, B. Yuan, X. Lai, X. Yan, Z.F. Ren, *Mater. Res. Bull.* **2016**, *76*, 107.

[45] X. Shi, L. Chen, C. Uher, *Int. Mater. Rev.* **2016**, *61*, 379.

[46] J.R. Sootsman, D.Y. Chung, M.G. Kanatzidis, *Angew. Chem., Int. Ed.* **2009**, *48*, 8616.

[47] C.G. Fu, S.Q. Bai, Y.T. Liu, Y.S. Tang, L.D. Chen, X.B. Zhao, T.J. Zhu, *Nat. Commun.* **2015**, *6*.

[48] T.J. Zhu, C.G. Fu, H.H. Xie, Y.T. Liu, X.B. Zhao, *Adv. Energy Mater.* **2015**, *5*.

[49] W. Li, G.F. Yang, J.W. Zhang, *J. Phys. D: Appl. Phys.* **2016**, *49*.

[50] Q.Y. Xue, H.J. Liu, D.D. Fan, L. Cheng, B.Y. Zhao, J. Shi, *Phys. Chem. Chem. Phys.* **2016**, *18*, 17912.

[51] P. Gao, I. Berkun, R.D. Schmidt, M.F. Luzenski, X. Lu, P. Bordon Sarac, E.D. Case, T.P. Hogan, *J. Electron. Mater.* **2014**, *43*, 1790.

[52] M.B.A. Bashir, S. Mohd Said, M.F.M. Sabri, D.A. Shnawah, M.H. Elsheikh, *Renewable Sustainable Energy Rev.* **2014**, *37*, 569.

[53] L.D. Zhao, S.H. Lo, Y. Zhang, H. Sun, G. Tan, C. Uher, C. Wolverton, V.P. Dravid, M.G. Kanatzidis, *Nature.* **2014**, *508*, 373.

[54] N. Mateeva, H. Niculescu, J. Schlenoff, L. Testardi, *J. Appl. Phys.* **1998**, *83*, 3111.

[55] O.T. Ikkala, L.O. Pietilä, L. Ahjopalo, H. Österholm, P.J. Passiniemi, *J. Chem. Phys.* **1995**, *103*, 9855.

[56] G.H. Kim, D.H. Hwang, S.I. Woo, *Phys. Chem. Chem. Phys.* **2012**, *14*, 3530.

[57] K. Xu, G. Chen, D. Qiu, *J. Mater. Chem. A.* **2013**, *1*, 12395.

[58] M. Culebras, C.M. Gómez, A. Cantarero, *J. Mater. Sci.* **2013**, *48*, 2855.

[59] M. Piao, G. Kim, G.P. Kennedy, S. Roth, U. Dettlaff-Weglikowska, *Phys. Status Solidi B.* **2013**, *250*, 2529.

[60] W. Lee, Y.H. Kang, J.Y. Lee, K.S. Jang, S.Y. Cho, *RSC Adv.* **2016**, *6*, 53339.

[61] N. Toshima, S. Ichikawa, *J. Electron. Mater.* **2015**, *44*, 384.

[62] K.C. See, J.P. Feser, C.E. Chen, A. Majumdar, J.J. Urban, R.A. Segalman, *Nano Lett.* **2010**, *10*, 4664.

[63] E.J. Bae, Y.H. Kang, K.S. Jang, S.Y. Cho, *Sci. Rep.* **2016**, *6*.

[64] D. Yoo, J. Kim, J.H. Kim, *Nano Res.* **2014**, *7*, 717.

[65] Y. Xuan, X. Liu, S. Desbief, P. Leclère, M. Fahlman, R. Lazzaroni, M. Berggren, J. Cornil, D. Emin, X. Crispin, *Phys. Rev. B.* **2010**, *82*, 115454.

[66] K. Bender, E. Gogu, I. Hennig, D. Schweitzer, H. Müenstedt, *Synth. Met.* **1987**, *18*, 85.

[67] N. Dubey, M. Leclerc, *J. Polym. Sci., Part B: Polym. Phys.* **2011**, *49*, 467.

[68] C. Gao, G. Chen, *Compos. Sci. Technol.* **2016**, *124*, 52.

[69] G.H. Kim, L. Shao, K. Zhang, K.P. Pipe, *Nat. Mater.* **2013**, *12*, 719.

[70] R.M. Ireland, H.E. Katz, *Innovative Thermoelectric Materials: Polymer, Nanostructure and Composite Thermoelectrics*, Imperial College Press **2016**.

[71] B. Zhang, J. Sun, H.E. Katz, F. Fang, R.L. Opila, *ACS Appl. Mater. Interfaces.* **2010**, *2*, 3170.

[72] Q. Yao, L.D. Chen, W.Q. Zhang, S.C. Liufu, X.H. Chen, *ACS Nano.* **2010**, *4*, 2445.

[73] Q. Yao, Q. Wang, L.M. Wang, L.D. Chen, *Energy Environ. Sci.* **2014**, *7*, 3801.

[74] C. Cho, K.L. Wallace, P. Tzeng, J.H. Hsu, C. Yu, J.C. Grunlan, *Adv. Energy Mater.* **2016**, *6*.

[75] O. Bubnova, Z.U. Khan, H. Wang, S. Braun, D.R. Evans, M. Fabretto, P. Hojati-Talemi, D. Dagnelund, J.B. Arlin, Y.H. Geerts, S. Desbief, D.W. Breiby, J.W. Andreasen, R. Lazzaroni, W.M. Chen, I. Zozoulenko, M. Fahlman, P.J. Murphy, M. Berggren, X. Crispin, *Nat. Mater.* **2014**, *13*, 190.

[76] K. Lee, S. Cho, S.H. Park, A. Heeger, C.-W. Lee, S.-H. Lee, *Nature.* **2006**, *441*, 65.

[77] T.C. Tsai, H.C. Chang, C.H. Chen, W.T. Whang, *Org. Electron.* **2011**, *12*, 2159.

[78] G.H. Kim, K.P. Pipe, *Innovative Thermoelectric Materials: Polymer, Nanostructure and Composite Thermoelectrics*, Imperial College Press **2016**.

[79] J.J. Luo, D. Billep, T. Waechtler, T. Otto, M. Toader, O. Gordan, E. Sheremet, J. Martin, M. Hietschold, D.R.T. Zahnd, T. Gessner, *J. Mater. Chem. A.* **2013**, *1*, 7576.

[80] N. Massonnet, A. Carella, O. Jaudouin, P. Rannou, G. Laval, C. Celle, J.P. Simonato, *J. Mater. Chem. C.* **2014**, *2*, 1278.

[81] H. Park, S.H. Lee, F.S. Kim, H.H. Choi, I.W. Cheong, J.H. Kim, *J. Mater. Chem. A.* **2014**, *2*, 6532.

[82] C. Cho, B. Stevens, J.H. Hsu, R. Bureau, D.A. Hagen, O. Regev, C. Yu, J.C. Grunlan, *Adv. Mater.* **2015**, *27*, 2996.

[83] S. Bhadra, D. Khastgir, N.K. Singha, J.H. Lee, *Prog. Polym. Sci.* **2009**, *34*, 783.

[84] Q. Yao, Q. Wang, L.M. Wang, Y. Wang, J. Sun, H.R. Zeng, Z.Y. Jin, X.L. Huang, L.D. Chen, *J. Mater. Chem. A.* **2014**, *2*, 2634.

[85] B. Russ, M.J. Robb, F.G. Brunetti, P.L. Miller, E.E. Perry, S.N. Patel, V. Ho, W.B. Chang, J.J. Urban, M.L. Chabinyc, C.J. Hawker, R.A. Segalman, *Adv. Mater.* **2014**, *26*, 3473.

[86] K. Walzer, B. Männig, M. Pfeiffer, K. Leo, *Chem. Rev.* **2007**, *107*, 1233.

[87] C.K. Mai, R.A. Schlitz, G.M. Su, D. Spitzer, X. Wang, S.L. Fronk, D.G. Cahill, M.L. Chabinyc, G.C. Bazan, *J. Am. Chem. Soc.* **2014**, *136*, 13478.

[88] I. Vlassiouk, G. Polizos, R. Cooper, I. Ivanov, J.K. Keum, F. Paulauskas, P. Datskos, S. Smirnov, *ACS Appl. Mater. Interfaces.* **2015**, *7*, 10702.

[89] P. Avouris, *Nano Lett.* **2010**, *10*, 4285.

[90] N. Tombros, A. Veligura, J. Junesch, J. Jasper Van Den Berg, P.J. Zomer, M. Wojtaszek, I.J. Vera Marun, H.T. Jonkman, B.J. Van Wees, *J. Appl. Phys.* **2011**, *109*.

[91] C. Berger, Z. Song, T. Li, X. Li, A.Y. Ogbazghi, R. Feng, Z. Dai, N. Alexei, M.E.H. Conrad, P.N. First, W.A. De Heer, *Journal of Physical Chemistry B.* **2004**, *108*, 19912.

[92] A.A. Balandin, S. Ghosh, W. Bao, I. Calizo, D. Teweldebrhan, F. Miao, C.N. Lau, *Nano Lett.* **2008**, *8*, 902.

[93] L. Wang, X. Lu, S. Lei, Y. Song, *J. Mater. Chem. A.* **2014**, *2*, 4491.

[94] T. Vuorinen, J. Niittynen, T. Kankkunen, T.M. Kraft, M. Mäntysalo, *Sci. Rep.* **2016**, *6*.

[95] W. Wang, Q. Zhang, J. Li, X. Liu, L. Wang, J. Zhu, W. Luo, W. Jiang, *RSC Adv.* **2015**, *5*, 8988.

[96] K.T. Kim, S.Y. Choi, E.H. Shin, K.S. Moon, H.Y. Koo, G.-G. Lee, G.H. Ha, *Carbon.* **2013**, *52*, 541.

[97] M.A. Kamarudin, S.R. Sahamir, R.S. Datta, B.D. Long, M.F. Mohd Sabri, S. Mohd Said, *The Scientific World Journal.* **2013**, *2013*.

[98] B. Madavali, H.S. Kim, M.G. Choi, G.C. Park, J.M. Koo, H.T. Son, S.J. Hong, *International Journal of Applied Ceramic Technology.* **2015**.

[99] D. Kim, Y. Kim, K. Choi, J.C. Grunlan, C.H. Yu, *ACS Nano.* **2010**, *4*, 513.

[100] Y. Du, S.Z. Shen, K.F. Cai, P.S. Casey, *Prog. Polym. Sci.* **2012**, *37*, 820.

[101] A. Dey, A. Maity, M.A.S. Khan, A.K. Sikder, S. Chattopadhyay, *RSC Adv.* **2016**, *6*, 22453.

[102] D.J. Bergman, O. Levy, *J. Appl. Phys.* **1991**, *70*, 6821.

[103] N.E. Coates, S.K. Yee, B. McCulloch, K.C. See, A. Majumdar, R.A. Segalman, J.J. Urban, *Adv. Mater.* **2013**, *25*, 1629.

[104] J.J. Urban, N.E. Coates, *Innovative Thermoelectric Materials: Polymer, Nanostructure and Composite Thermoelectrics*, Imperial College Press **2016**.

[105] Y. Du, S.Z. Shen, W.D. Yang, R. Donelson, K.F. Cai, P.S. Casey, *Synth. Met.* **2012**, *161*, 2688.

[106] L.M. Wang, Q. Yao, H. Bi, F.Q. Huang, Q. Wang, L.D. Chen, *J. Mater. Chem. A.* **2015**, *3*, 7086.

[107] L.M. Wang, Q. Yao, H. Bi, F.Q. Huang, Q. Wang, L.D. Chen, *J. Mater. Chem. A.* **2014**, *2*, 11107.

[108] B. Abad, I. Alda, P. Diaz-Chao, H. Kawakami, A. Almarza, D. Amantia, D. Gutierrez, L. Aubouy, M. Martin-Gonzalez, *J. Mater. Chem. A.* **2013**, *1*, 10450.

[109] J.L. Xiang, L.T. Drzal, *Polymer.* **2012**, *53*, 4202.

[110] M. Mitra, C. Kulsi, K. Chatterjee, K. Kargupta, S. Ganguly, D. Banerjee, S. Goswamid, *RSC Adv.* **2015**, *5*, 31039.

[111] C.Z. Meng, C.H. Liu, S.S. Fan, *Adv. Mater.* **2010**, *22*, 535.

[112] Q.L. Zhang, W.J. Wang, J.L. Li, J.J. Zhu, L.J. Wang, M.F. Zhu, W. Jiang, *J. Mater. Chem. A.* **2013**, *1*, 12109.

[113] H. Wang, S.I. Yi, X. Pu, C. Yu, *ACS Appl. Mater. Interfaces.* **2015**, *7*, 9589.

[114] Q. Wang, Q. Yao, J. Chang, L.D. Chen, *J. Mater. Chem.* **2012**, *22*, 17612.

[115] J.L. Liu, J. Sun, L. Gao, *Nanoscale.* **2011**, *3*, 3616.

[116] Z. Tian, S. Lee, G. Chen, *Journal of Heat Transfer.* **2013**, *135*, 061605.

[117] C. Suter, P. Tomeš, A. Weidenkaff, A. Steinfeld, *Materials.* **2010**, *3*, 2735.

[118] L. Chen, J. Gong, F. Sun, C. Wu, *International journal of thermal sciences.* **2002**, *41*, 95.

[119] Y. Pei, N.A. Heinz, G.J. Snyder, *Journal of Materials Chemistry.* **2011**, *21*, 18256.

[120] A. Shakouri, *Materials Research.* **2011**, *41*, 399.

[121] M.S. Hossain, F. Al-Dirini, F.M. Hossain, E. Skafidas, *Scientific reports.* **2015**, *5*.

[122] B.V.K. Reddy, M. Barry, J. Li, M.K. Chyu, *J. Heat Trans.-T. Asme.* **2014**, *136*.

[123] J.W. Stevens, *Energy Conversion and Management.* **2001**, *42*, 709.

[124] S. LeBlanc, *Sustainable Materials and Technologies.* **2014**, *1*, 26.

[125] X. Hu, A. Yamamoto, M. Ohta, H. Nishiate, *Review of Scientific Instruments.* **2015**, *86*, 045103.

[126] H.-H. Hsu, C.-H. Cheng, Y.-L. Lin, S.-H. Chiou, C.-H. Huang, C.-P. Cheng, *Applied Physics Letters.* **2013**, *103*, 053902.

[127] H.-H. Hsu, C.-H. Cheng, S.-H. Chiou, C.-H. Huang, C.-M. Liu, Y.-L. Lin, W.-H. Chao, P.-H. Yang, C.-Y. Chang, C.-P. Cheng, *Journal of Alloys and Compounds.* **2014**, *588*, 633.

[128] M.K. Kim, M.S. Kim, S. Lee, C. Kim, Y.J. Kim, *Smart Mater. Struct.* **2014**, *23*.

[129] Z.S. Lu, H.H. Zhang, C.P. Mao, C.M. Li, *Appl. Energy.* **2016**, *164*, 57.

[130] Y. Du, K. Cai, S. Chen, H. Wang, S.Z. Shen, R. Donelson, T. Lin, *Sci. Rep.* **2015**, *5*.

[131] D.X. Liang, H.R. Yang, S.W. Finefrock, Y. Wu, *Nano Lett.* **2012**, *12*, 2140.

[132] S.W. Finefrock, X.Q. Zhu, Y.M. Sun, Y. Wu, *Nanoscale.* **2015**, *7*, 5598.

[133] R. Bjork, D.V. Christensen, D. Eriksen, N. Pryds, *Int. J. Therm. Sci.* **2014**, *85*, 12.

[134] J.H. Meng, X.X. Zhang, X.D. Wang, *Int. J. Heat Mass Transfer.* **2015**, *80*, 227.

[135] M. Chen, L.A. Rosendahl, T. Condra, *Int. J. Heat Mass Transfer.* **2011**, *54*, 345.

[136] G. Fraisse, J. Ramousse, D. Sgorlon, C. Goupil, *Energy Convers. Manage.* **2013**, *65*, 351.

[137] A. Bejan, *Heat transfer handbook* A. Bejan, A.D. Kraus (Eds.), John Wiley & Sons, **2003**.

[138] R. Vallabh, P. Banks-Lee, M. Mohammadi, *J. Eng. Fibers Fabr.* **2008**, *3*, 46.

[139] G.C. Zhu, D. Kremenakova, Y. Wang, J. Militky, R. Mishra, *Text. Res. J.* **2015**, *85*, 1681.

[140] S.D. Cimilli, E. Deniz, C. Candan, B.U. Nergis, *Fibres Text. East. Eur.* **2012**, *20*, 42.

[141] Y. Li, Q. Zhu, K.W. Yeung, *Text. Res. J.* **2002**, *72*, 435.

[142] D. Bhattacharjee, V.K. Kothari, *J. Text. Inst.* **2008**, *99*, 433.

[143] M. Mohammadi, P. Banks-Lee, P. Ghadimi, *Text. Res. J.* **2003**, *73*, 896.

[144] I. Qashou, H.V. Tafreshi, B. Pourdeyhimi, *J. Eng. Fibers Fabr.* **2009**, *4*, 9.

[145] V.K. Kothari, D. Bhattacharjee, *J. Text. Inst.* **2008**, *99*, 421.

[146] D. Ding, T. Tang, G.W. Song, A. McDonald, *Text. Res. J.* **2011**, *81*, 945.

[147] C.O. Yoon, M. Reghu, D. Moses, A.J. Heeger, Y. Cao, *Phys. Rev. B.* **1993**, *48*, 14080.

[148] K.-C. Chang, M.-S. Jeng, C.-C. Yang, Y.-W. Chou, S.-K. Wu, M.A. Thomas, Y.-C. Peng, *J. Electron. Mater.* **2009**, *38*, 1182.

[149] S. Liu, N. Peng, Y. Bai, D.Y. Ma, F. Ma, K.W. Xu, *RSC Adv.* **2016**, *6*, 31668.

[150] K. Kusagaya, H. Hagino, S. Tanaka, K. Miyazaki, M. Takashiri, *J. Electron. Mater.* **2015**, *44*, 1632.

[151] J.P. Carmo, L.M. Goncalves, R.F. Wolffenbuttel, J.H. Correia, *Sens. Actuators, A.* **2010**, *161*, 199.

[152] L.M. Goncalves, P. Alpuim, G. Min, D.M. Rowe, C. Couto, J.H. Correia, *Vacuum.* **2008**, *82*, 1499.

[153] L.M. Goncalves, C. Couto, P. Alpuim, A.G. Rolo, F. Volklein, J.H. Correia, *Thin Solid Films.* **2010**, *518*, 2816.

[154] J.H. We, S.J. Kim, B.J. Cho, *Energy.* **2014**, *73*, 506.

[155] S.J. Kim, J.H. We, B.J. Cho, *Energy & Environmental Science.* **2014**, *7*, 1959.

[156] S.J. Kim, H.E. Lee, H. Choi, Y. Kim, J.H. We, J.S. Shin, K.J. Lee, B.J. Cho, *ACS nano.* **2016**, *10*, 10851.

[157] P.J. Taylor, *Materials, Preparation, and Characterization in Thermoelectrics* D.M. Rowe (Ed.) **2012**.

[158] W.R. Fahrner, S. Schwertheim, *Semiconductor Thermoelectric Generators*, Trans Tech, **2009**.

[159] L.J. Van der Pauw, *Philips Res. Rep.* **1958**, *13*, 1.

[160] G.S. Nolas, J. Sharp, J. Goldsmid, *Thermoelectrics: basic principles and new materials developments*, Springer Science & Business Media, **2001**.

[161] L.J. Van der Pauw, *Philips Tech. Rev.* **1958/1958**, *20*.

[162] D. Huzel, H. Reith, M. Schmitt, *Materials, Preparation, and Characterization in Thermoelectrics* D.M. Rowe (Ed.) **2012**.

[163] R. Taylor, *CRC handbook of thermoelectrics* D.M. Rowe (Ed.), CRC Press **1995**.

[164] D.G. Cahill, R.O. Pohl, *Phys. Rev. B.* **1987**, *35*, 4067.

[165] D.G. Cahill, H.E. Fischer, T. Klitsner, E. Swartz, R. Pohl, *J. Vac. Sci. Technol., A.* **1989**, *7*, 1259.

[166] T. Harman, *J. Appl. Phys.* **1958**, *29*, 1373.

[167] H. Goldsmid, *J. Thermoelectr.* **2006**, *1*, 5.

[168] S.M. Lin, J.L. Yu, *Int. J. Refrig.* **2016**, *65*, 103.

[169] H.S. Dizaji, S. Jafarmadar, S. Khalilarya, A. Moosavi, *Appl. Energy.* **2016**, *181*, 357.

[170] B.L. Huang, C. Lawrence, A. Gross, G.S. Hwang, N. Ghafouri, S.W. Lee, H. Kim, C.P. Li, C. Uher, K. Najafi, M. Kaviany, *J. Appl. Phys.* **2008**, *104*.

[171] W. He, G. Zhang, X.X. Zhang, J. Ji, G.Q. Li, X.D. Zhao, *Appl. Energy*. **2015**, *143*, 1.

[172] D.L. Zhao, G. Tan, *Appl. Therm. Eng.* **2014**, *66*, 15.

[173] P.C. Hsu, A.Y. Song, P.B. Catrysse, C. Liu, Y.C. Peng, J. Xie, S.H. Fan, Y. Cui, *Science.* **2016**, *353*, 1019.

[174] H.J. Goldsmid, *CRC handbook of thermoelectrics* D.M. Rowe (Ed.), CRC Press **1995**.

[175] G.L. Bennett, *CRC handbook of thermoelectrics* D.M. Rowe (Ed.), CRC Press **1995**.

[176] J.H. Yang, T. Caillat, *MRS Bull.* **2006**, *31*, 224.

[177] W.C. Hall, *CRC handbook of thermoelectrics* D.M. Rowe (Ed.), CRC Press **1995**.

[178] D. Kraemer, B. Poudel, H.P. Feng, J.C. Caylor, B. Yu, X. Yan, Y. Ma, X.W. Wang, D.Z. Wang, A. Muto, K. McEnaney, M. Chiesa, Z.F. Ren, G. Chen, *Nat. Mater*. **2011**, *10*, 532.

[179] K.S. Thomas, H.J. McMann, *US spacesuits*, Springer Science & Business Media, **2011**.

[180] K. Tanaka, K. Nakamura, T. Katafuchi, *Acta Astronautica.* **2014**, *104*, 260.

[181] W.S. Liu, Q. Jie, H.S. Kim, Z.F. Ren, *Acta Mater.* **2015**, *87*, 357.

[182] J. Yang, F.R. Stabler, *J. Electron. Mater.* **2009**, *38*, 1245.

[183] K. Ebrahimi, G.F. Jones, A.S. Fleischer, *Renewable Sustainable Energy Rev.* **2014**, *31*, 622.

[184] V. Leonov, R.J.M. Vullers, *J. Electron. Mater.* **2009**, *38*, 1491.

[185] S.M.A. Marouf, M.A.A. Eldosoky, Y.H. Ghallab, Ieee, *2015 27th International Conference on Microelectronics* **2015**.

[186] A.I. Casian, Sanduleac, II, *3rd International Conference on Nanotechnologies and Biomedical Engineering* V. Sontea, I. Tiginyanu (Eds.) **2016**.

[187] A. Cadei, A. Dionisi, E. Sardini, M. Serpelloni, *Meas. Sci. Technol.* **2014**, *25*.

[188] Y. Yang, X.J. Wei, J. Liu, *J. Phys. D: Appl. Phys.* **2007**, *40*, 5790.

[189] A.B. Amar, A.B. Kouki, H. Cao, *Sensors.* **2015**, *15*, 28889.

[190] X. Wei, J. Liu, *Front. Energy Power Eng. China.* **2008**, *2*, 1.

[191] J.H. Bahk, H. Fang, K. Yazawa, A. Shakouri, *J. Mater. Chem. C.* **2015**, *3*, 10362.

[192] V. Leonov, P. Fiorini, S. Sedky, T. Torfs, C. Van Hoof, International Conference on Solid State Sensors and Actuators and Microsystems, 2005

[193] Z. Wang, V. Leonov, P. Fiorini, C. Van Hoof, TRANSDUCERS and EUROSENSORS '07 - 4th International Conference on Solid-State Sensors, Actuators and Microsystems, 2007

[194] Z. Wang, V. Leonov, P. Fiorini, C. Van Hoof, *Sens. Actuators, A.* **2009**, *156*, 95.

[195] Z. Wang, P. Fiorini, V. Leonov, C. Van Hoof, *J. Micromech. Microeng.* **2009**, *19*.

[196] M. Wahbah, M. Alhawari, B. Mohammad, H. Saleh, M. Ismail, *IEEE J Em. Sel. Top. C.* **2014**, *4*, 354.

[197] F. Suarez, A. Nozariasbmarz, D. Vashaee, M.C. Ozturk, *Energy Environ. Sci.* **2016**, *9*, 2099.

[198] X. Yan, G. Joshi, W. Liu, Y. Lan, H. Wang, S. Lee, J.W. Simonson, S.J. Poon, T.M. Tritt, G. Chen, Z.F. Ren, *Nano Lett.* **2011**, *11*, 556.

[199] X. Yan, W. Liu, H. Wang, S. Chen, J. Shiomi, K. Esfarjani, H. Wang, D. Wang, G. Chen, Z. Ren, *Energy Environ. Sci.* **2012**, *5*, 7543.

[200] J.H. Li, Q. Tan, J.F. Li, D.W. Liu, F. Li, Z.Y. Li, M.M. Zou, K. Wang, *Adv. Funct. Mater.* **2013**, *23*, 4317.

[201] D.W. Xie, J.T. Xu, G.Q. Liu, Z. Liu, H.Z. Shao, X.J. Tan, J. Jiang, H.C. Jiang, *Energies.* **2016**, *9*.

[202] L.P. Hu, H.J. Wu, T.J. Zhu, C.G. Fu, J.Q. He, P.J. Ying, X.B. Zhao, *Adv. Energy Mater.* **2015**, *5*.

[203] Y.D. Liu, X.H. Li, Q. Zhang, C. Chen, J.H. Li, L. Zhang, D.L. Yu, Y.J. Tian, B. Xu, *J. Mater. Sci.: Mater. Electron.* **2016**, *27*, 6433.

[204] D.K. Shin, I.H. Kim, *J. Electron. Mater.* **2016**, *45*, 1234.

[205] X.H. Li, Q. Zhang, Y.L. Kang, C. Chen, L. Zhang, D.L. Yu, Y.J. Tian, B. Xu, *J. Alloys Compd.* **2016**, *677*, 61.

[206] J. Navratil, T. Plechacek, C. Drasar, V. Kucek, F. Laufek, E. Cernoskova, L. Benes, M. Vlcek, *J. Electron. Mater.* **2016**, *45*, 2904.

[207] L.W. Fu, J.Y. Yang, Q.H. Jiang, Y. Xiao, Y.B. Luo, D. Zhang, Z.W. Zhou, *J. Electron. Mater.* **2016**, *45*, 1240.

[208] K.M. Song, D.K. Shin, I.H. Kim, *J. Electron. Mater.* **2016**, *45*, 1227.

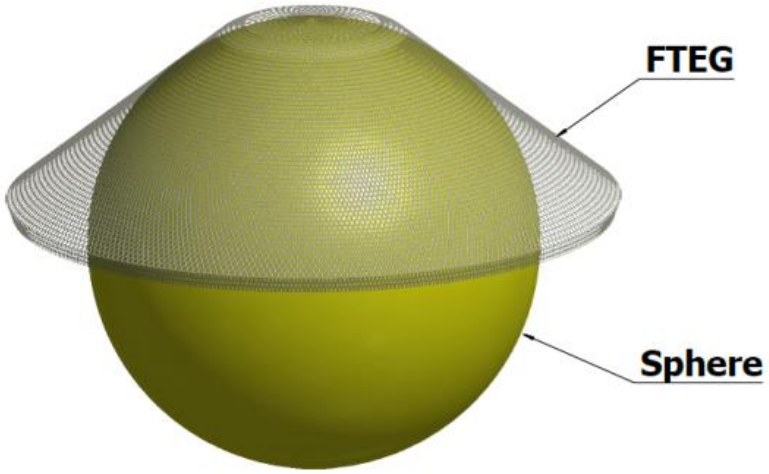

(a)

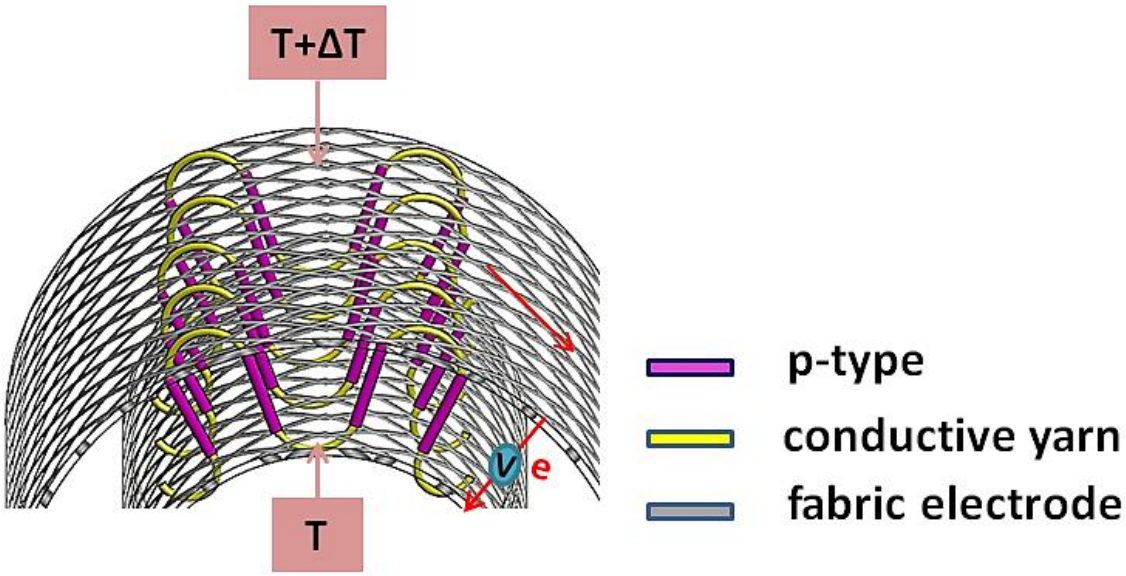

(b)

Figure 1. A typical FTEG draped on a sphere (a) and enlarged view of the device structure (b)

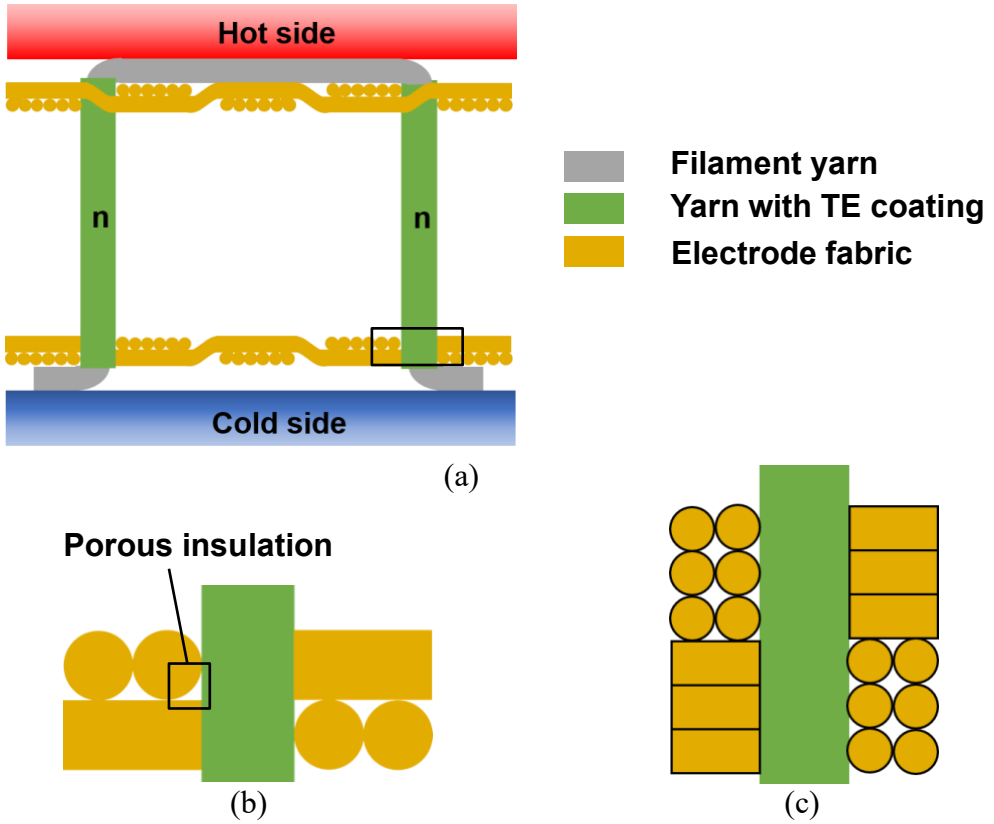

Figure 2. (a) Schema of a typical FTEG unit. (b) and (c) the enlarged contact regions between the electrode fabric and TE coated yarns.

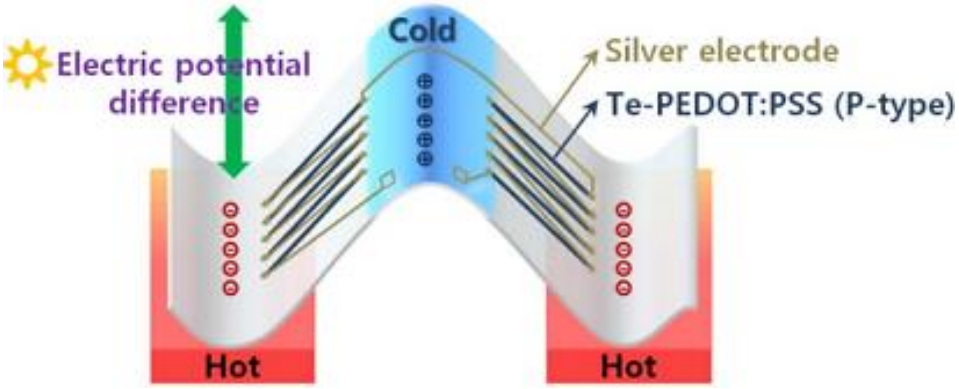

Figure 3. Schematic diagram of geometric configuration of a TE generator.[63]

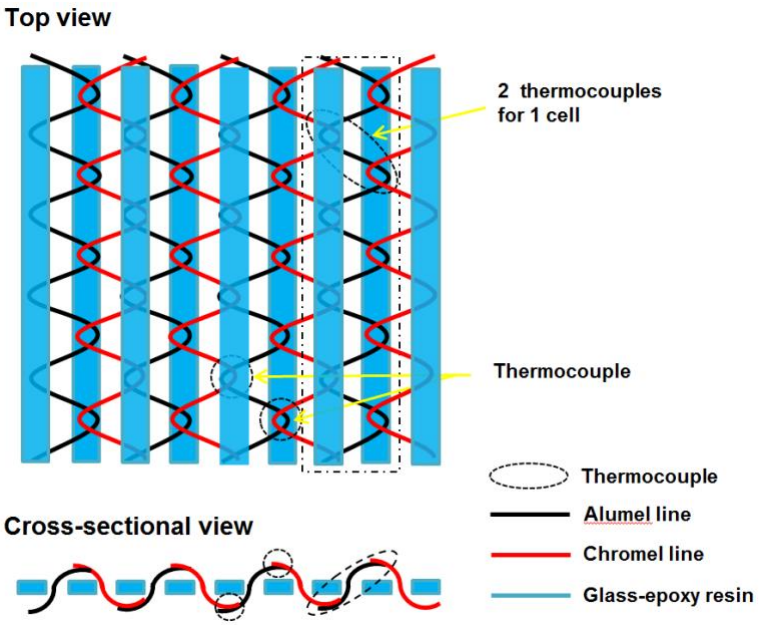

Figure 4. Schema of knitted panel

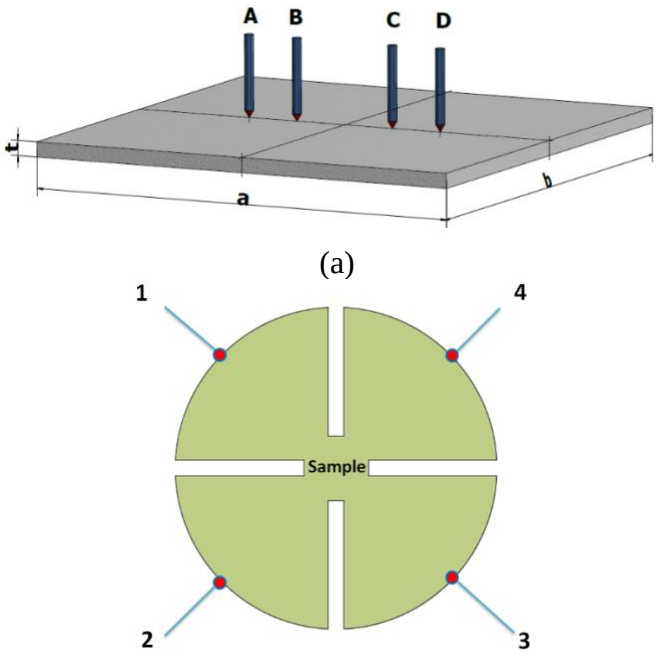

Figure 5. (a) Schema of a four-point probe method: A~D represent 4 probes; (b) the preferred contact placements of van der Pauw's method: 1~4.

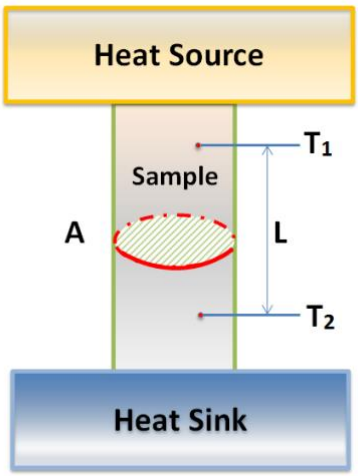

Figure 6. Schema of measuring thermal conductivity with a steady-state technique.

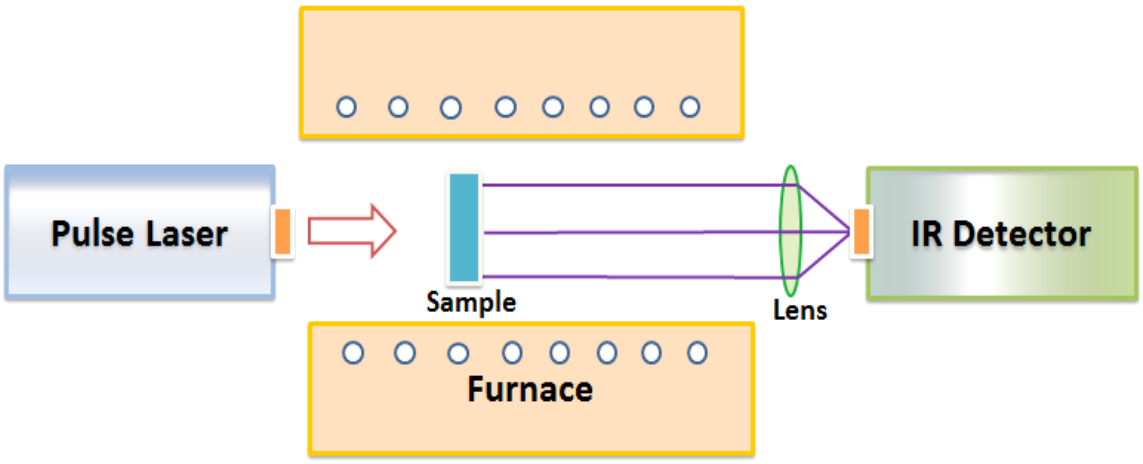

Figure 7. Schema of laser flash method

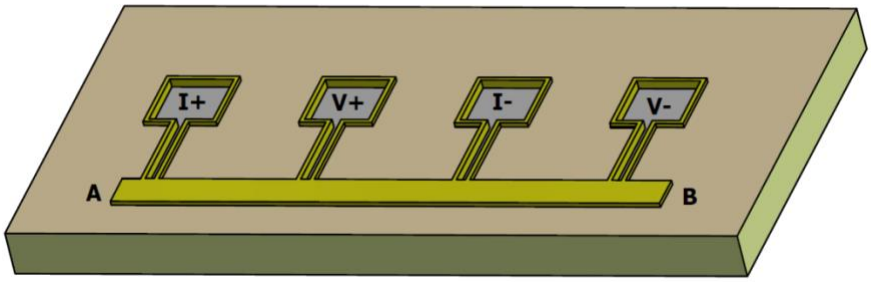

Figure 8. Schema of 3ω method: line AB is a metal strip acting as a heater and a thermometer simultaneously.

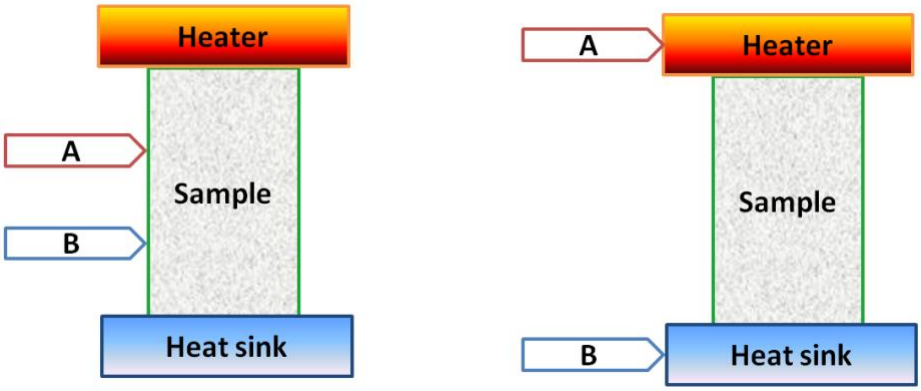

(a) (b)

Figure 9. Schema of measuring Seebeck coefficient: (a) the measurement points of thermocouples contact with samples directly; (b) the measurement points of thermocouples contact with heater and heat sink.

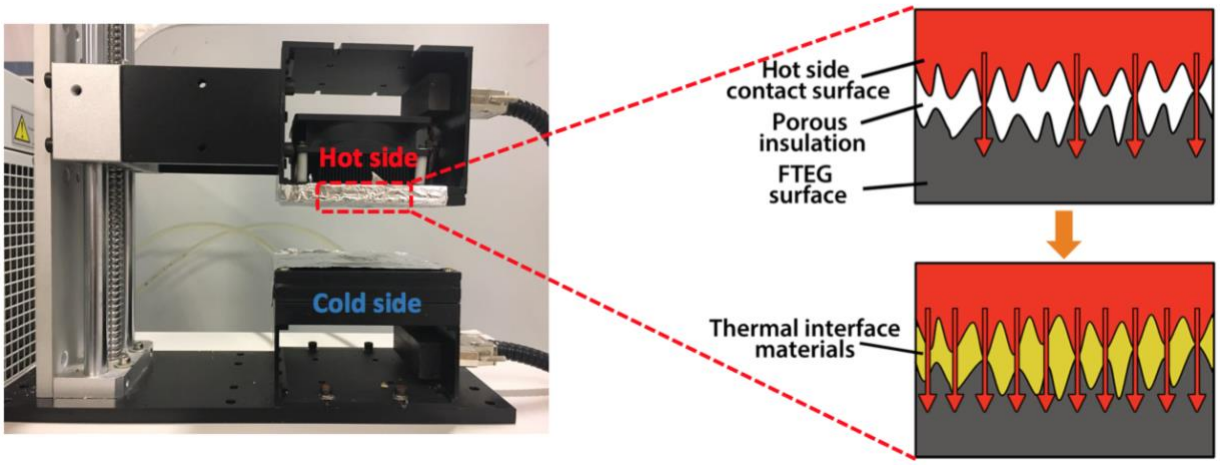

Figure 10. A lab-made experimental set-up for TE properties of FTEGs.

Table 1. Summary of some popular inorganic TE materials: types, highest ZT values at different temperature

Inorganic TE materials		Type	*ZT*	Power factor (mW/(m·K^2))	Temperature (K)	Ref.
Half-Heusler (HH) compound	$Hf_{0.75}Zr_{0.25}NiSn_{0.975}Sb_{0.025}$	n-type	~0.8	––	1025	[48]
	$Hf_{0.6}Zr_{0.4}NiSn_{0.98}Sb_{0.02}$	n-type	~1.0	––	1000	[48]
	$Hf_{0.6}Zr_{0.4}NiSn_{0.99}Sb_{0.01}$	n-type	~1.0	––	873~973	[48]
	0.2%Sb-doped $Ti_{0.5}Zr_{0.25}Hf_{0.25}NiSn$	n-type	1.2	––	830	[48]
	$Zr_{0.5}Hf_{0.5}CoSb_{0.8}Sn_{0.2}$	p-type	0.8	~2.8	973	[198]
	$Hf_{0.8}Ti_{0.2}CoSb_{0.8}Sn_{0.2}$	p-type	1.0	~2.6	1073	[199]
	$FeNb_{0.86}Hf_{0.14}Sb$	p-type	~1.5	––	1200	[47]
	$FeNb_{0.88}Hf_{0.12}Sb$	p-type	~1.5	––	1200	[47]
Bi-Te Alloy	$Bi_xSb_{2-x}Te_3$	p-type	1.4	~4.8	373	[36]
	$Bi_{0.3}Sb_{1.7}Te_3$	p-type	1.33	~3.4	373	[200]
	$Bi_{0.5}Sb_{1.5}Te_3$	p-type	1.86±0.15	––	320	[37]
	$Bi_{0.48}Sb_{1.52}Te_3$/0.05 wt% Graphene	p-type	1.25	4.8	320	[201]
	$Bi_2Te_{2.79}Se_{0.21}$	n-type	1.2	––	357	[202]
Skutterudite compounds	$Co_{3.2}Fe_{0.8}Sb_{12}$	p-type	0.53	~1.8	823	[203]
	$Nd_{0.9}Fe_{3.5}Co_{0.5}Sb_{12}$	p-type	0.91	~3.0	723	[204]
	$Ca_{0.31}Co_4Sb_{12}$	p-type	1.15	5.4	840	[205]
	$FeSb_2Te_{0.85}Sn_{0.15}$		0.47	––	673	[206]
	$CeFe_4Sb_{11.9}Te_{0.1}$	p-type	0.76	––	773	[207]
	$La_{0.75}Pr_{0.25}Fe_4Sb_{12}$	p-type	0.83	3.1	823	[208]
	$La_{0.75}Pr_{0.25}Fe_{3.75}Co_{0.25}Sb_{12}$	p-type	0.81	3.1	723	[208]